--- Soufriere Hills Eruption ---

表面現象:

Dome-collapse と Vulcanian explosion に伴う

地震、火砕流、噴出物(堆積物)の特徴

2008.01.18 & 25 火山物理セミナー

火山センター　前野 深

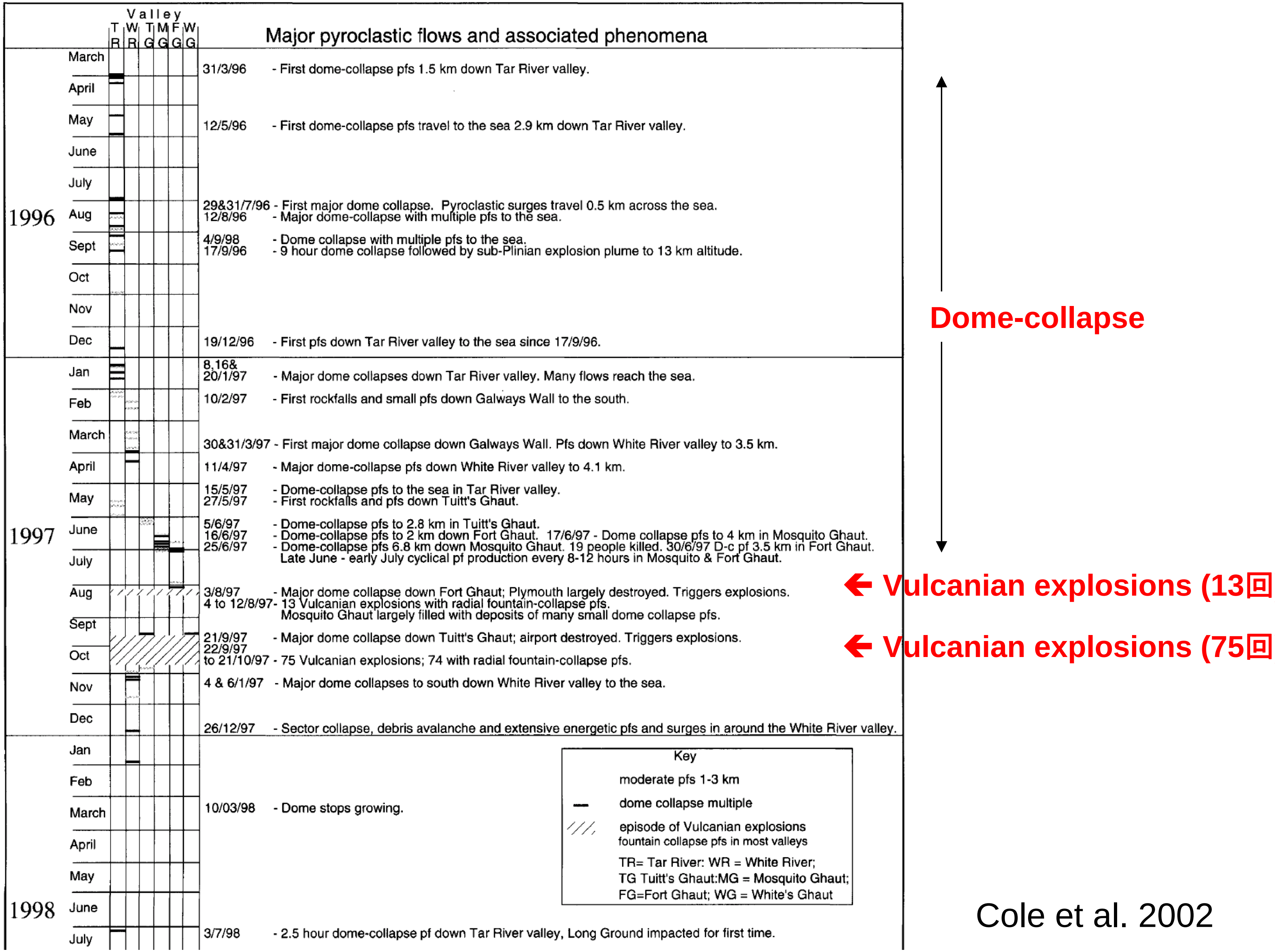

Cole et al. 2002

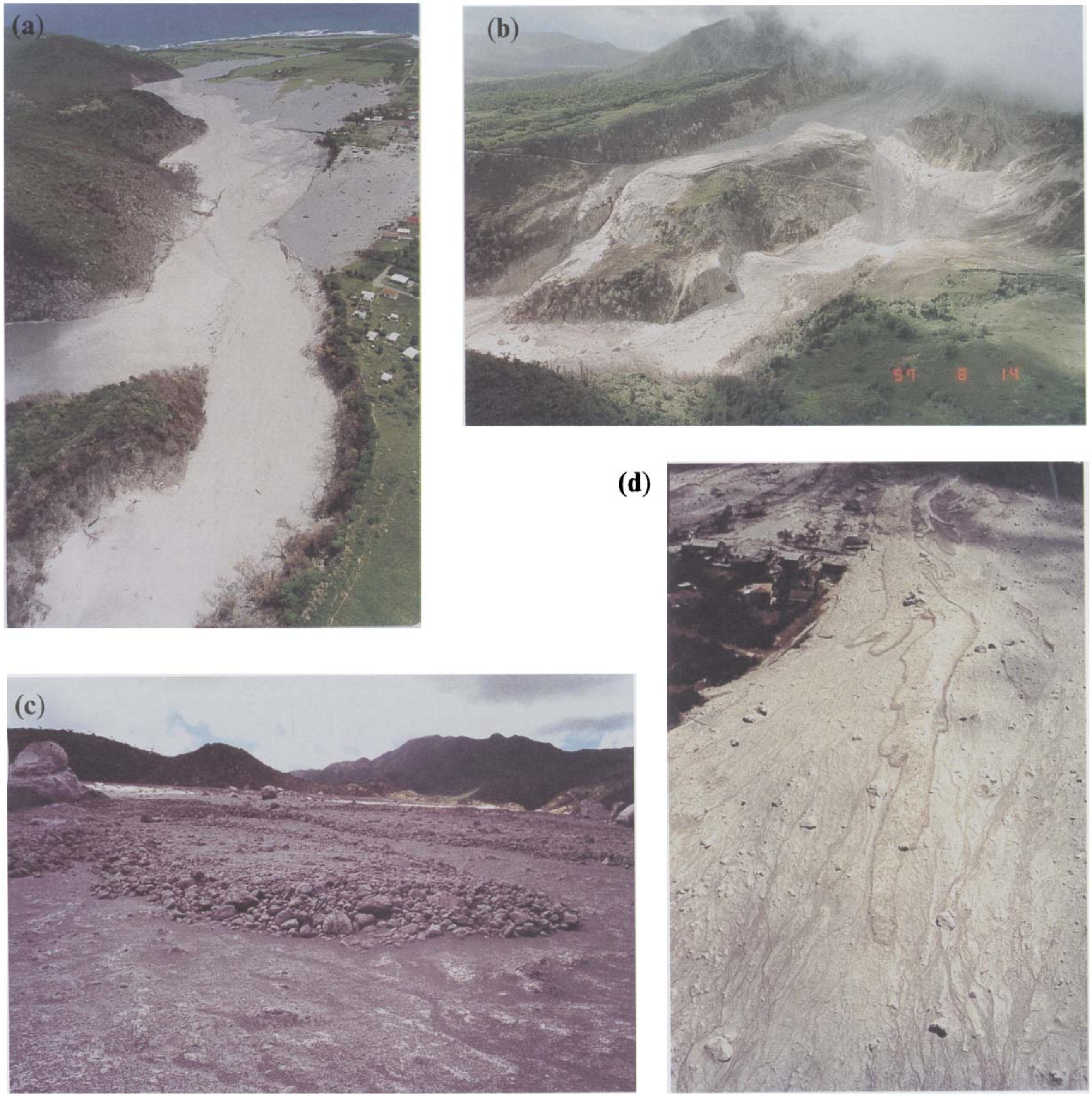

Druitt et al. 2002

1996-1999 噴火で発生した Pyroclastic density currents の種類

(1) Dome-collapse flows (small or large)

(2) Surges

(3) Derived flows (Secondary pyroclastic flows)

(4) Pumice-rich flows (by Fountain-collapse)

Flow type	*Date*	*H* (km)	*L* (km)	*V* (x 10^6 m^3)	*A* (x 10^6 m^2)
i) dome-collapse flows	3-Apr-96	0.59 ± 0.03	1.60 ± 0.04	0.152	0.101
	12-May-96	0.91 ± 0.03	2.90 ± 0.04	0.331	0.175
	31-Mar-97	0.86 ± 0.03	2.50 ± 0.04	0.163	0.109
	5-Jun-97	0.86 ± 0.03	3.10 ± 0.04	0.375	0.192
	17-June-97	0.86 ± 0.03	3.90 ± 0.04	0.766	0.300
	25-Jun-97	1.01 ± 0.03	6.70 ± 0.04	5.538	0.784
	30-Mar-97	0.83 ± 0.03	3.60 ± 0.04	2.600	0.160
	11-Apr-97	0.90 ± 0.03	4.05 ± 0.04	2.900	0.430
	3-Aug-97	0.90 ± 0.03	5.60 ± 0.04	8.750	1.784
	21-Sep-97	0.92 ± 0.03	6.00 ± 0.04	13.563	2.357
ii) surges	25-Jun-97	1.01 ± 0.03	6.70 ± 0.05	0.791	3.954
	26-Dec-97	1.20 ± 0.03	5.00 ± 0.05	2.500	9.794
iii) derived flows	25-Jun-97	0.26 ± 0.1	4.00 ± 0.15	0.087	0.262
	26-Dec-97	0.51 ± 0.1	3.00 ± 0.15	0.053	0.511
iv) pumice-rich flows	18-Oct-97	1.22 ± 0.1	4.60 ± 0.15	0.141	0.471
	18-Oct-97	1.27 ± 0.1	4.40 ± 0.15	0.082	0.272
	18-Oct-97	1.05 ± 0.1	3.00 ± 0.15	0.020	0.066
	18-Oct-97	1.11 ± 0.1	3.30 ± 0.15	0.063	0.209

The pumice flow data is the product of a single explosion where the flows in different directions are considered as 4 individual events.

Calder et al. (1999)

Mobility of Flows

Calder et al. 1999

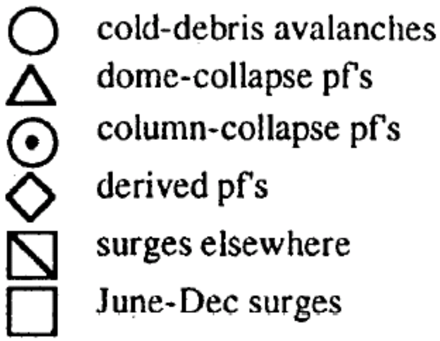

$$\frac{A}{V^{\frac{2}{3}}} = \lambda^{\frac{1}{3}} \left(\frac{\rho g H}{\tau} \right)^{\frac{2}{3}}$$

(Dade and Huppert, 1998)

τ: Average shear stress in the mobile debris

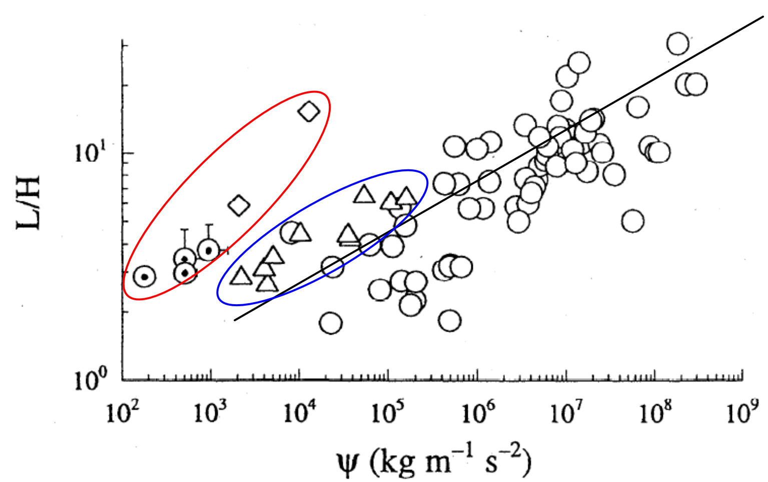

Inundated area

Mobility parameter

Plan-shape parameter (=A/L^2) [the ratio of the average width to the length of an avalanche deposit]

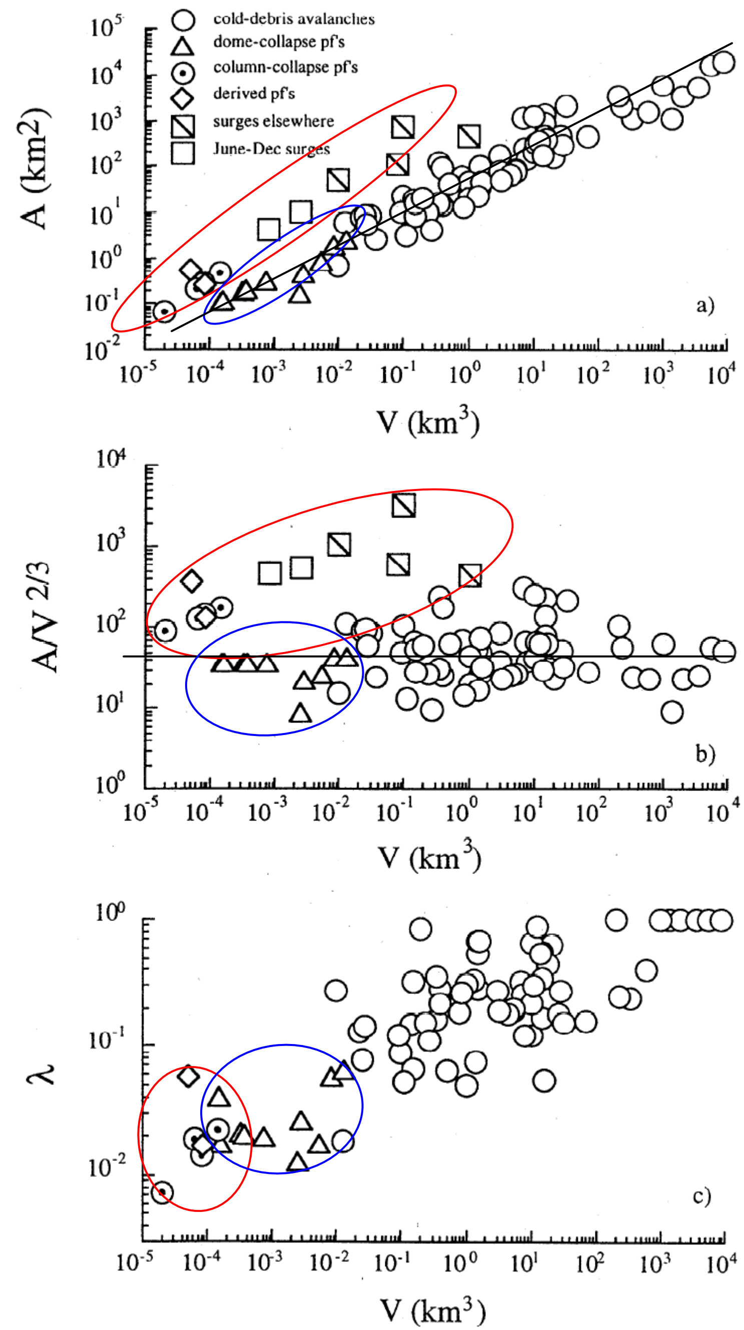

[参考文献]

Dome collapse events and flows

Robertson et al. (1998) The explosive eruption of Soufriere Hills Volcano, Montserrat, West Indies, 17 September, 1996. GRL.

Cole et al. (1998) Pyroclastic flows generated by gravitational instability of the 1996-97 lava dome of Soufriere Hills Volcano, Montserrat. GRL.

Calder et al. (1999) Mobility of pyroclastic fows at the Soufrie're Hills Volcano, Montserrat. GRL.

Calder et al. (2002) Mechanisms of lava dome instability and generation of rockfalls and pyroclastic fows at Soufrie're Hills Volcano, Montserrat. GSL Memoirs.

Cole et al. (2002) Deposits from dome-collapse and fountain-collapse pyroclastic fows at Soufrie're Hills Volcano, Montserrat. GSL Memoirs.

Druitt et al. (2002) Small volume, highly mobile pyroclastic fows formed by rapid sedimentation from pyroclastic surges at Soufrie're Hills Volcano, Montserrat: an important volcanic hazard. GSL Memoirs.

Luckett et al. (2002) The relationship between degassing and rockfall signals at Soufriere Hills Volcano, Montserrat. GSL Memoirs.

Fountain-collapse events and flows

Druitt et al. (2002) Episodes of cyclic Vulcanian explosive activity with fountain collapse at Soufrie're Hills Volcano, Montserrat. GSL Memoirs.

Formenti and Druitt (2003) Vesicle connectivity in pyroclasts and implications for the fluidisation of fountain-collapse pyroclastic flows, Monserrat (West Indies), EPSL.

Formenti et al. (2003) Characterisation of the 1997 Vulcanian explosions of Soufrire Hills Volcano, Montserrat, by video analysis. Bull Volcanol.

Calder et al. 2002, GSL Memoirs

Mechanisms of lava dome instability
and generation of rockfalls and
pyroclastic flows

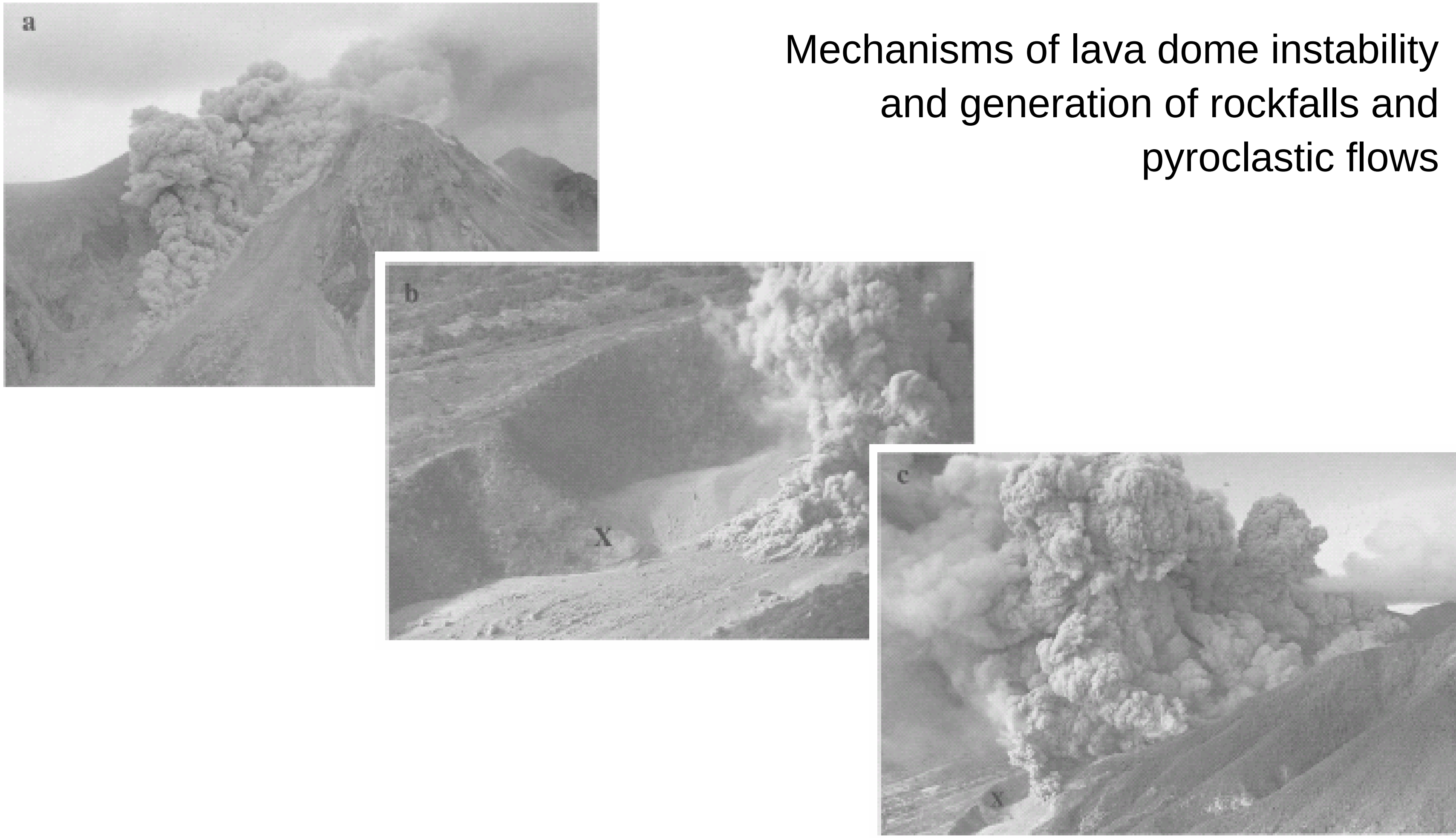

(1) 溶岩ドームの不安定化・崩壊の要因

(2) 溶岩ドーム崩壊と、火砕流発生・タイプとの関連

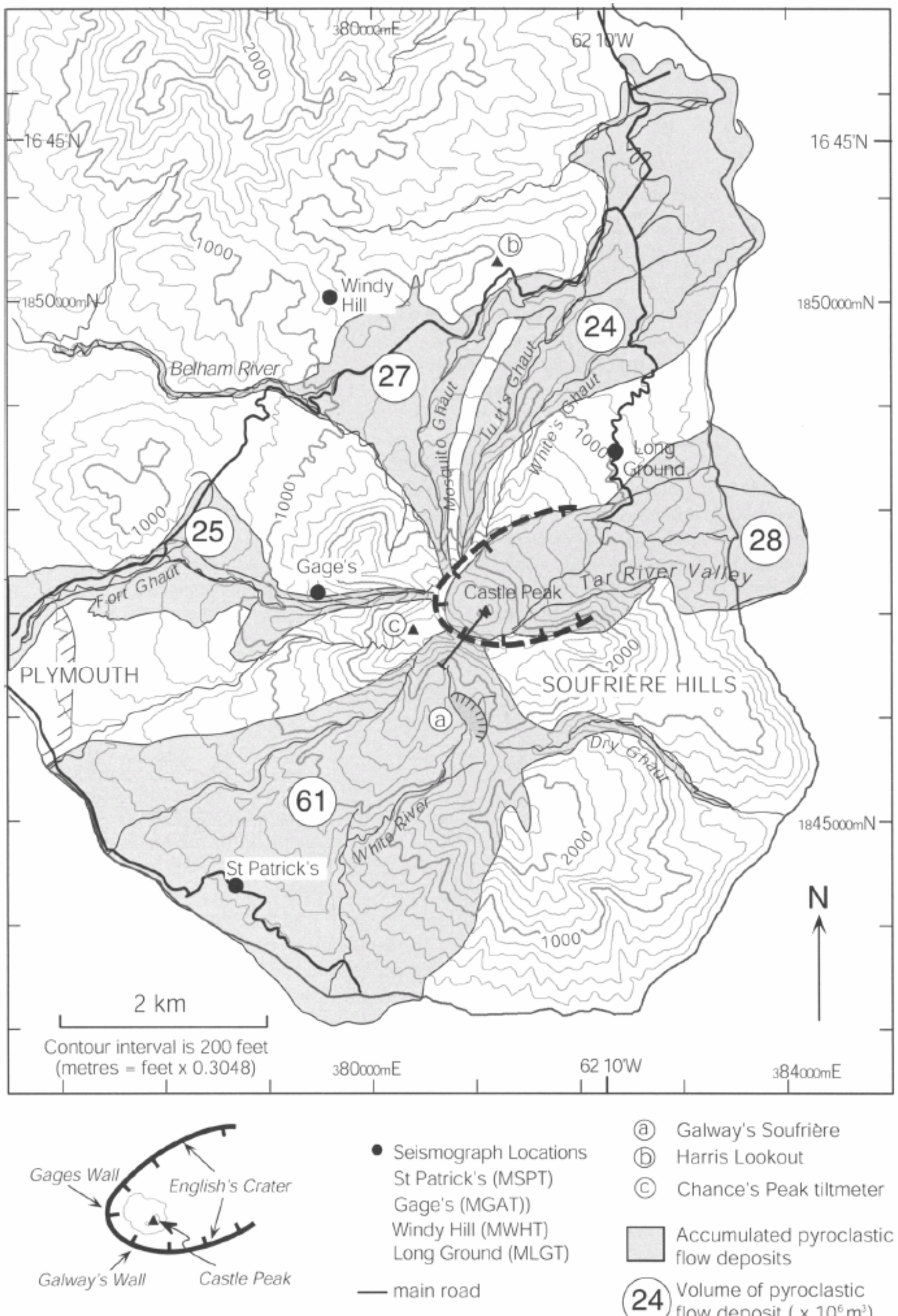

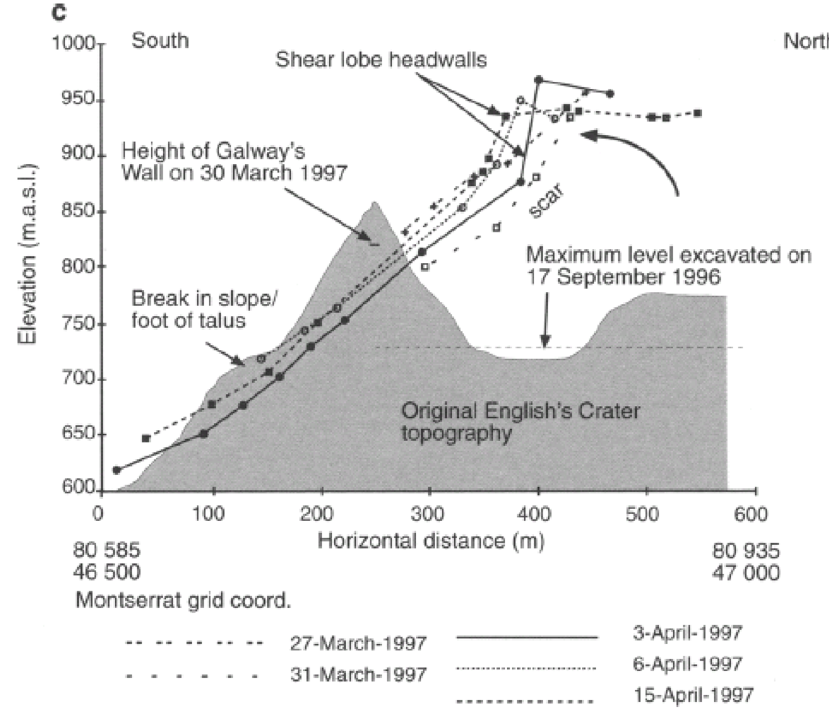

Fig. 1. Map of southern Montserrat with distribution of total accumulated (November 1995–March 1998) pyroclastic flow deposits. Topography exerted a major control on flow paths and, therefore, on the spatial development of the depositional fans over time (Cole *et al.* 2002). The volumes ($\times 10^6$ m^3) of pyroclastic flow material accumulated within each of the main drainage systems are given. The deposit volumes within the Tar River and White River valleys are underestimates of the actual volumes discharged in those directions, as many of the flows there entered the sea. Key locations, such as the positions of selected seismic stations (black dots) and the Chance's Peak tiltmeter, are given. English's Crater and the locations of Galway's Wall and Castle Peak are shown in the bottom left-hand corner. The section line through English's Crater wall marks the position of the section in Figure 6c.

Seismic signals

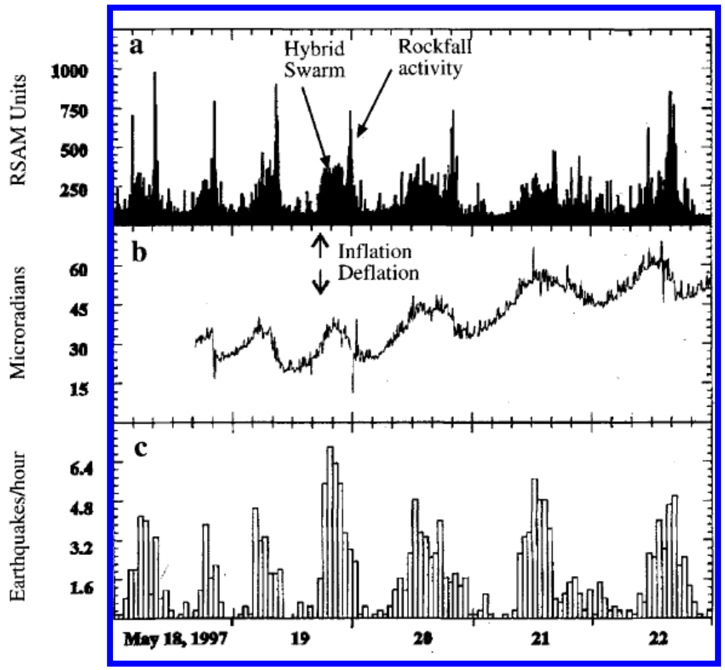

Fig. 5. Comparisons of (**a**) RSAM with (**b**) cyclic tilt records and (**c**) the total number of triggered earthquakes per hour for the period 18–22 May 1997. The triggered earthquakes are dominated by hybrid events that subsequently produce the cyclic, low-amplitude RSAM peaks. The large spikes in RSAM are rockfalls and small pyroclastic flows, produced at the onset of deflation. Spikes on tilt records represent noise (modified from Voight *et al.* 1998).

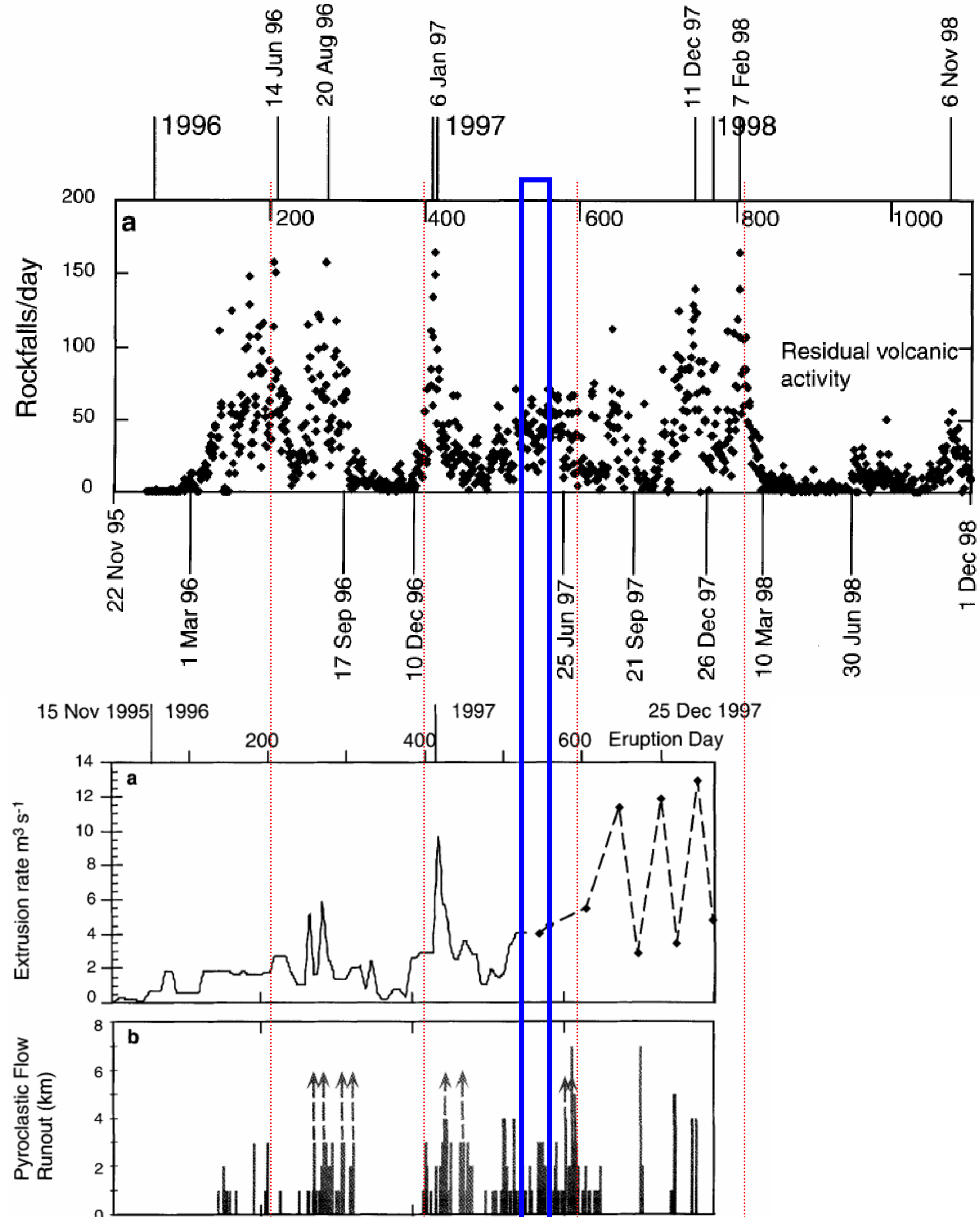

Rock fall と Pyroclastic flow の特徴 (Calder et al. 2002; Luckett et al. 2002)

合計 27150回の seismic signals (Rock falls and Pyroclastic flow)
Large (1- 4$\times 10^6$ km^3) and Major (> 4$\times 10^6$ km^3) dome collapse & Pfl generation
➔ 噴出率 6-13 m^3/s, hybrid-earthquake swarms, inflation-deflation cycles of ground deformation (下限: 2 m^3/s and 30$\times 10^6$ km^3)

Rockfall の回数と継続時間（duration）⇔ 噴出率と相関

Seismic signals: (Neuberg et al. 2000; Luckett et al. 2002)
1. Long-period (LP) components (1-2 Hz) ➔ Intense degassing from the lava dome
2. High-frequency components (2-8 Hz) ➔ Falling & flowing debris

Pulses of magma extrusion & Discharge of pressurized gas ➔ Cyclic actively dome failure
Hot & gas-rich, fragmentation of microvesicular andesite lava ➔ Pyroclastic flows

Event magnitude (Runout distance of pfl and Rockfall duration)
➔ **Power-law between Frequency vs. Magnitude**

Smaller flow と Larger flow

 # Smaller flows by discrete & single pulse collapse events [数回/day]

- Volume: 0.2×10^6 (DRE)
- Runout distance: < 3 km
- Flow velocity: 3 〜 10 m/s
- Slope: > 20° Erosion and deposition
- Dome extrusion rate: 1 〜 4 m^3/s
- Major deposits: **Coarse, block-rich deposits (limited ash-cloud surge facies)**

 # Larger flows by sustained collapse events [数回/月]

- Volume: 1 〜 9×10^6 (DRE)
- Runout distance: 3 〜 6.5 km
- Flow velocity: 15 〜 30 m/s
- Slope: 14 〜 16° (Erosion) ➔ 4 〜 6° (Deposition)
- Dome extrusion rate: 4 〜 10 m^3/s
- Major deposits: **Coarse block-rich deposits** & **Extensive, thin fine-grained ash**

Event magnitude for runout distance of pfl and rockfall duration)

Power law between Frequency vs. Magnitude

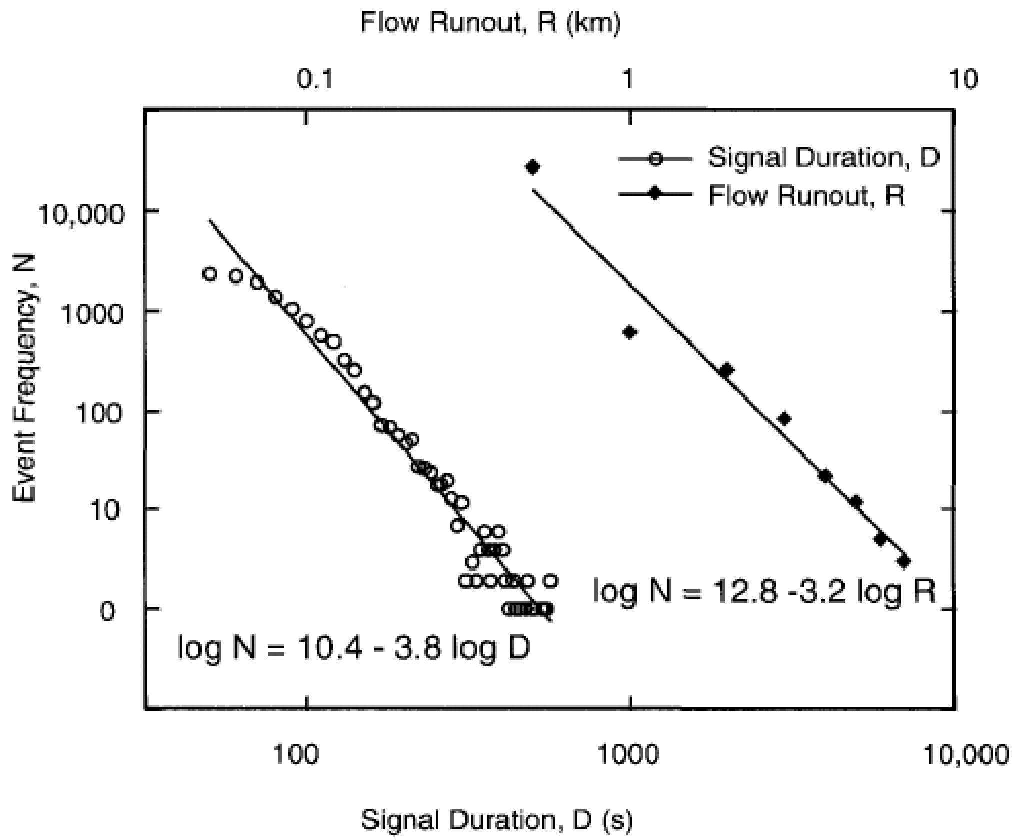

Fig. 13. Rockfall and pyroclastic flow frequency (in number of events, N) in relation to flow magnitude as determined by runout, R, for pyroclastic flows and seismic signal duration, D, for rockfalls.

Cole et al. 2002, GSL Memoirs

Deposits from dome-collapse and fountain-collapse pyroclastic fows

Block & ash flows from dome collapse

(a) Discrete small flow

(b) Discrete large flow

(c) Sustained-collapse larger flow

Pumice and ash flow from Vulcanian explosions (d)

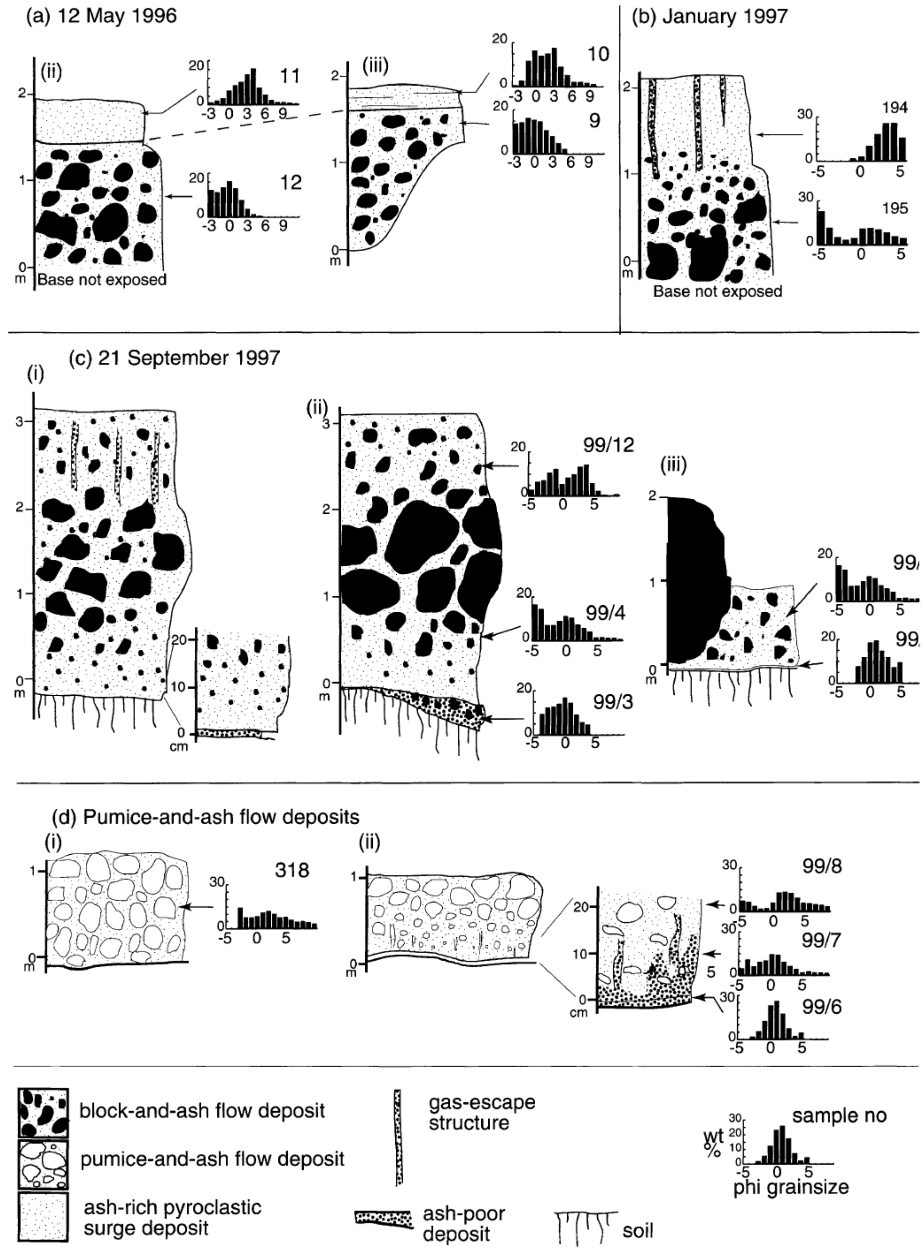

Fig. 11. Selected sections through block-and-ash flow deposits. (a) 12 May 1996 Tar River valley; (b) January 1997, Tar River fan; (c) 21 September 1997, north of Spanish Point; (d) pumice-and-ash flow deposits in Plymouth. Histograms show weight % versus phi size. For location of sections see Figures 2 and 6.

Cole et al. 2002

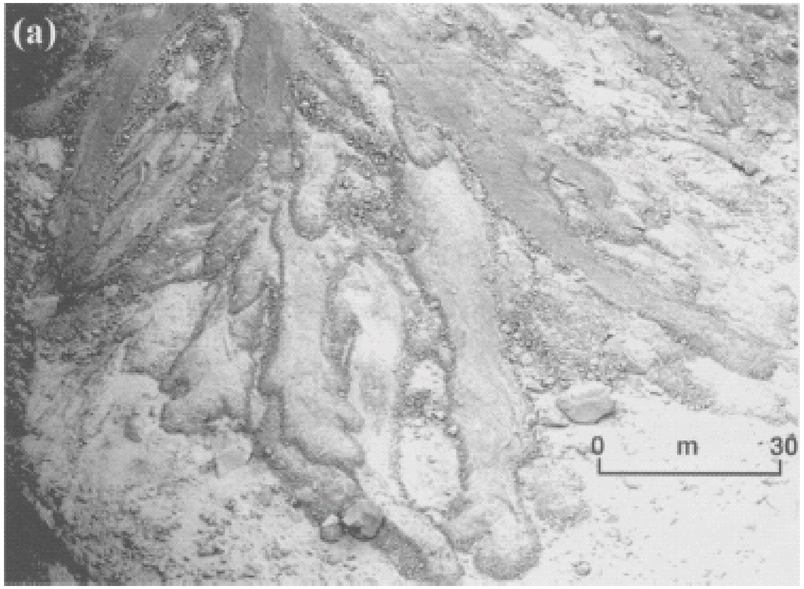

Lobes, levees, and channel morphology:
- Pumice & ash flows
- Small-volume block & ash flows

Ridge-and furrow surface morphology:
- Large-volume block & ash flows

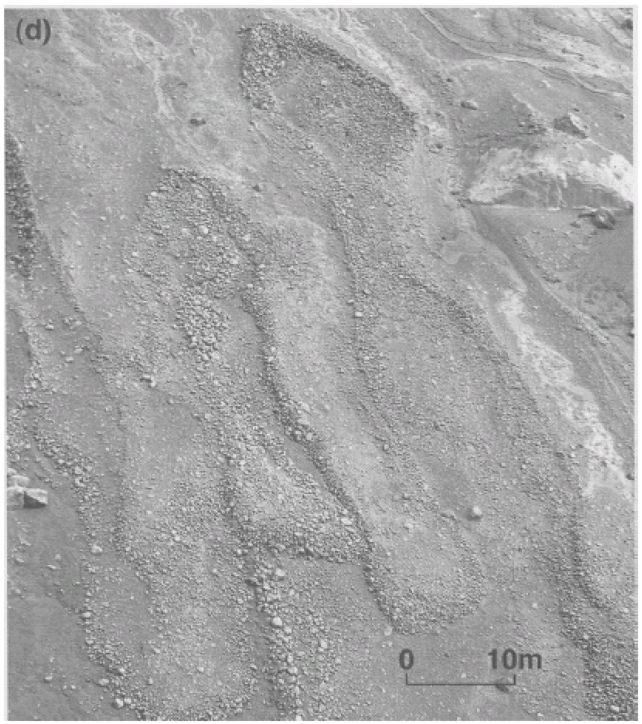

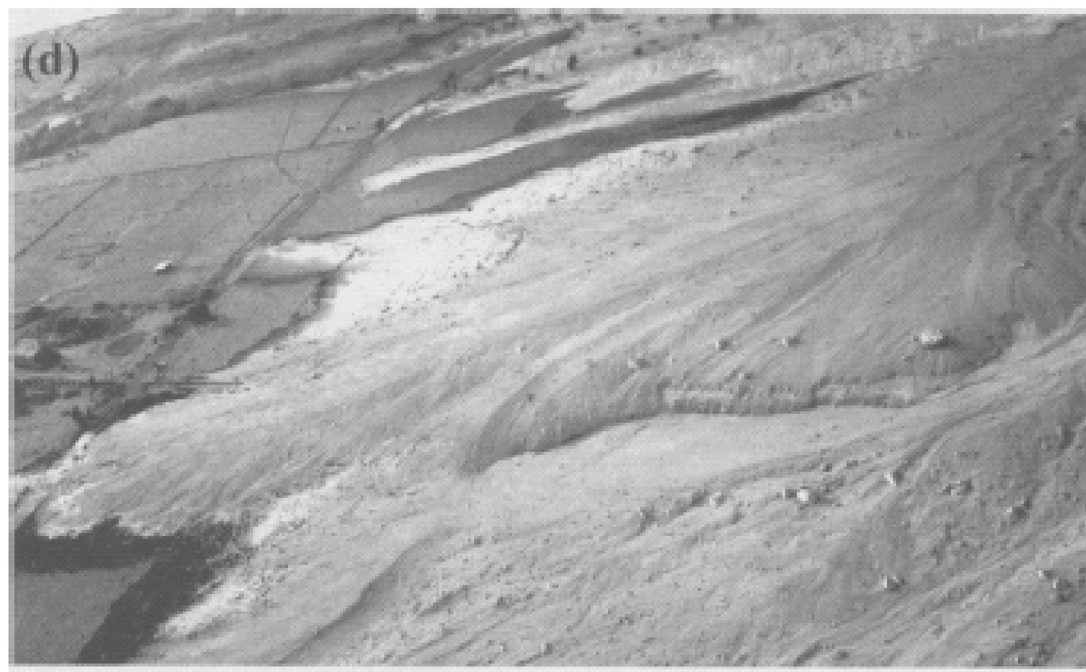

Large-volume block & ash flows

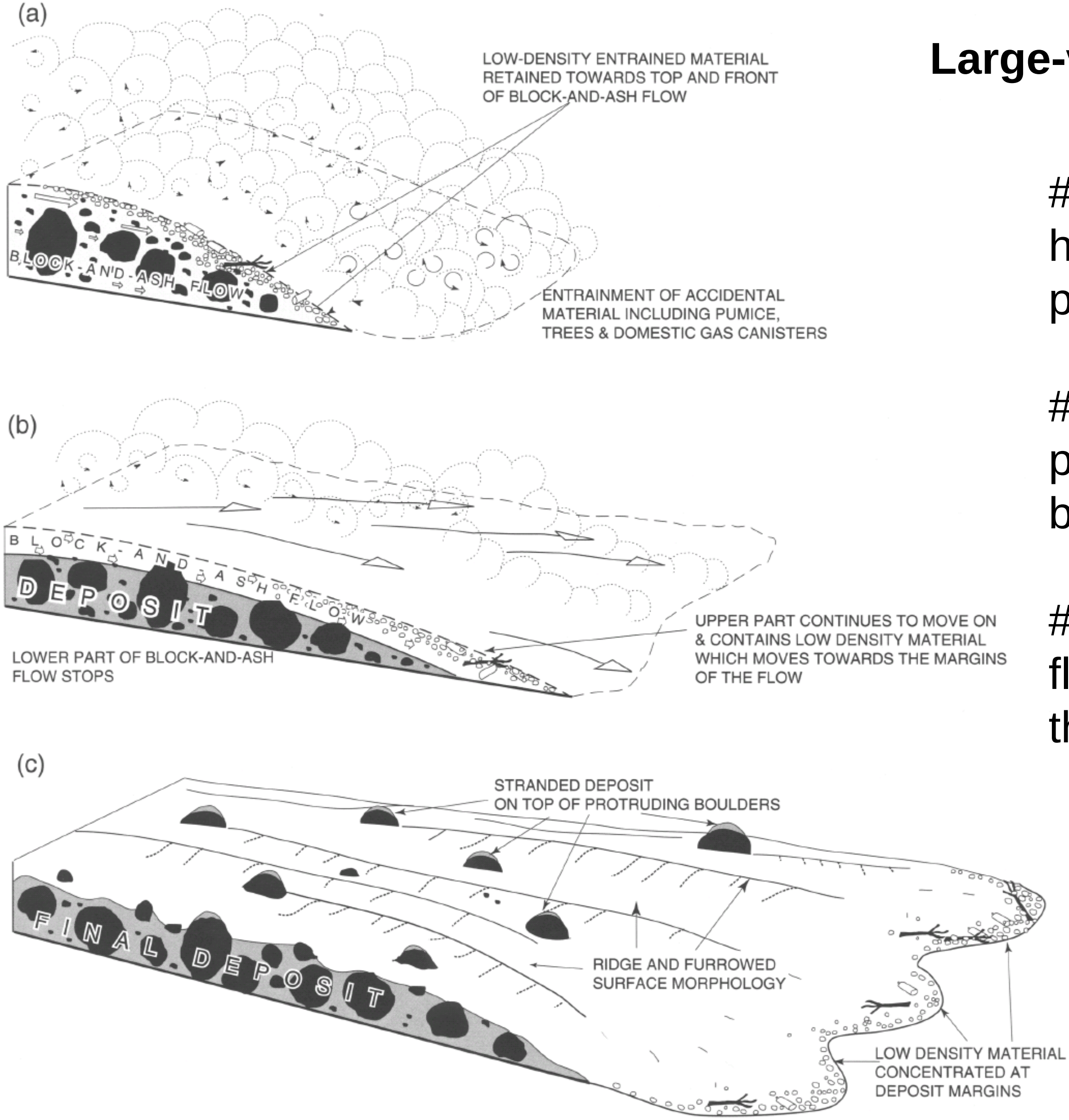

Fig. 22. Diagram summarizing the final stages of transport (*c.* 0.5 km) and emplacement of large-volume unconfined block-and-ash flow deposit. **(a)** Flow front entrains low-density material, which is concentrated towards the upper surface and front of the flow. **(b)** Lower part of the block-and-ash flow decelerates and comes to rest, whereas the upper part, containing the majority of low-density material, continues to move. **(c)** Final deposit is emplaced. Margins and front of the flow are rich in low-density material; upper surface of flow deposit has ridge-and-furrow morphology caused by motion of upper part of block-and-ash flow. Note deposit left stranded on top of boulders.

The upper part of the flow has detached from the lower part of the flow.

Remnants of the upper part were left on the top of boulders.

The moving pyroclastic flow was significantly thicker than the final deposit.

Cole et al. 2002

Calder et al. 1999

Inundated area

Geometric mobility parameter

Plane-shape parameter (=A/L²)

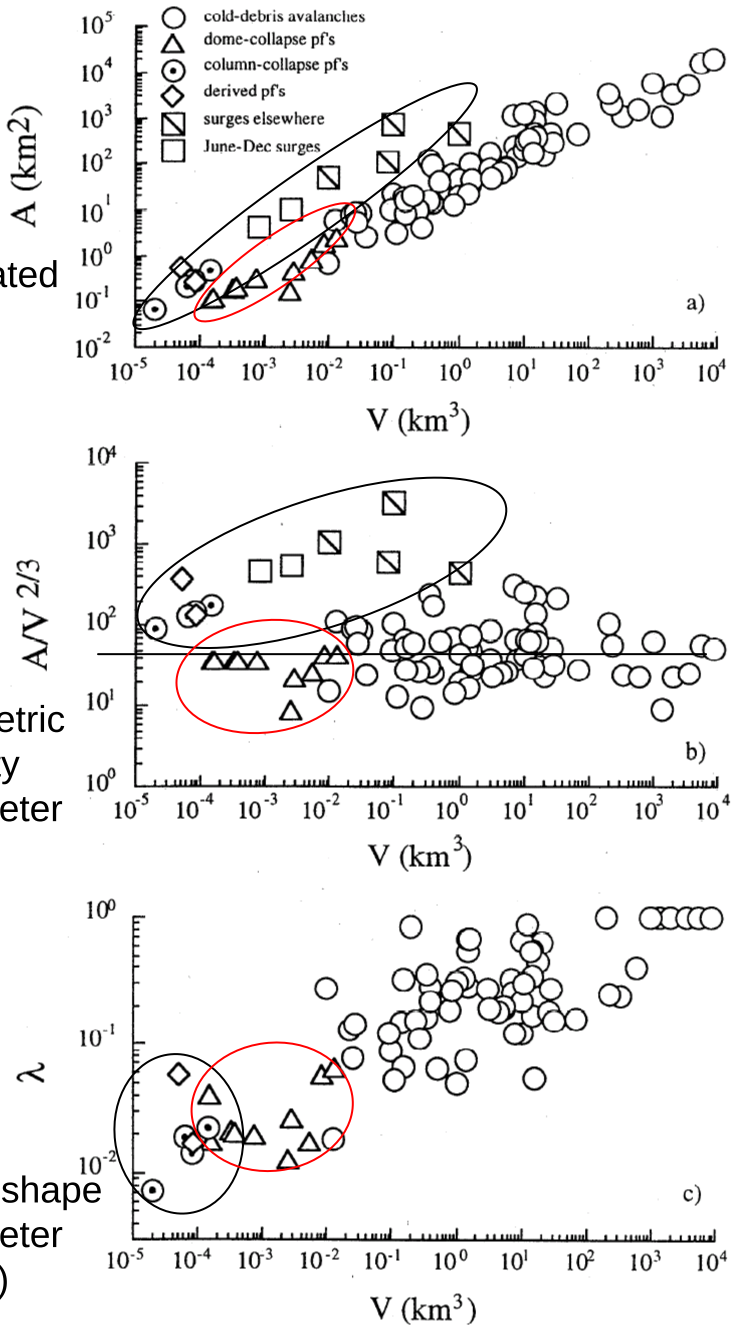

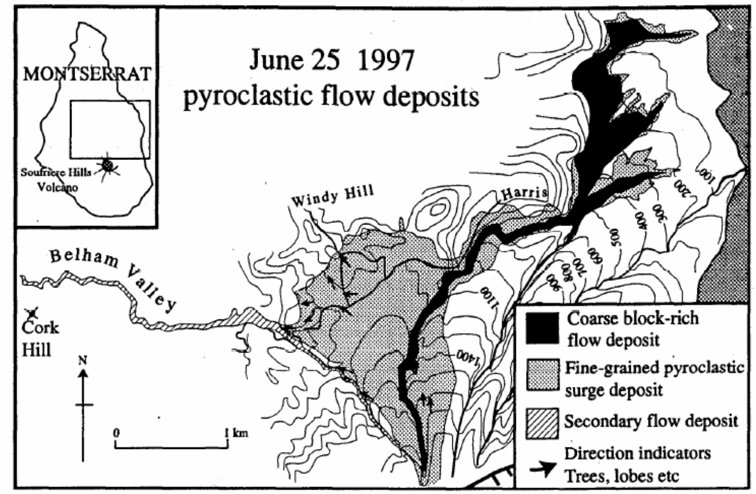

Figure 3. Map of the northern sector of Soufriere Hills Volcano, Montserrat, showing the routes of the main pyroclastic flow, surge and derivative pyroclastic flow of 25 June 1997.

Soufriere Hills の Block & ash flow の Mobility は、他の火山の Flow（図中: ○）とよく似た傾向を示すが、

- Column-collapse pyroclastic flow

- Derived (secondary) pyroclastic flow

-Surges

より小さいという特徴.

Druitt et al. (2002) Episodes of cyclic Vulcanian explosive activity with fountain collapse

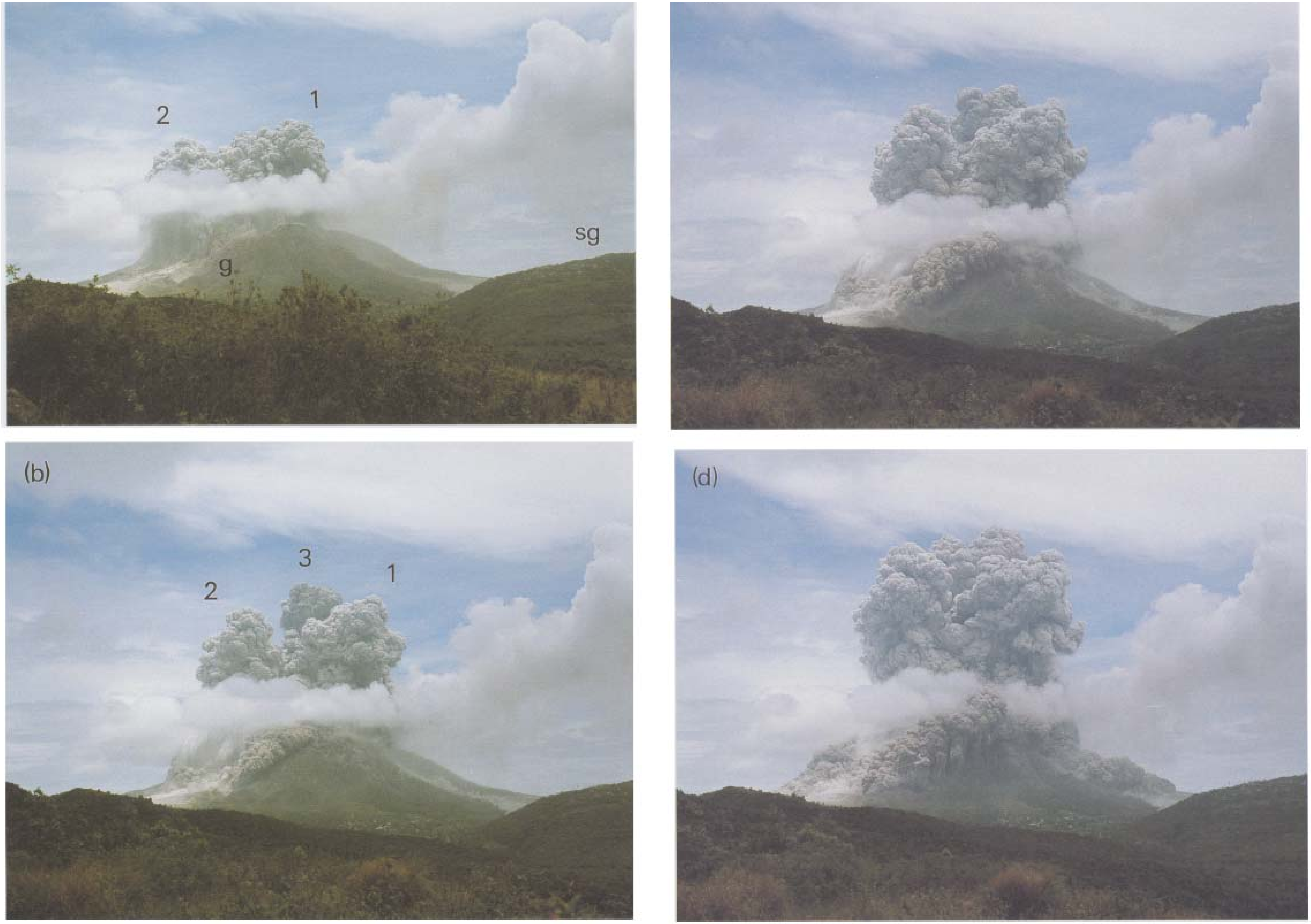

Fig. 6. Explosion at 15:13 on 20 October 1997. Fountain collapse generated pyroclastic surges and flows visible to the west (right) and north (left) of Gages Mountain (g). Ash was thrown up by the ground impact of ballistic blocks (b). The buoyant plume ultimately rose to about 10 km. Note the buildings for scale in the foreground. Photographs taken from the NW by P. Cole.

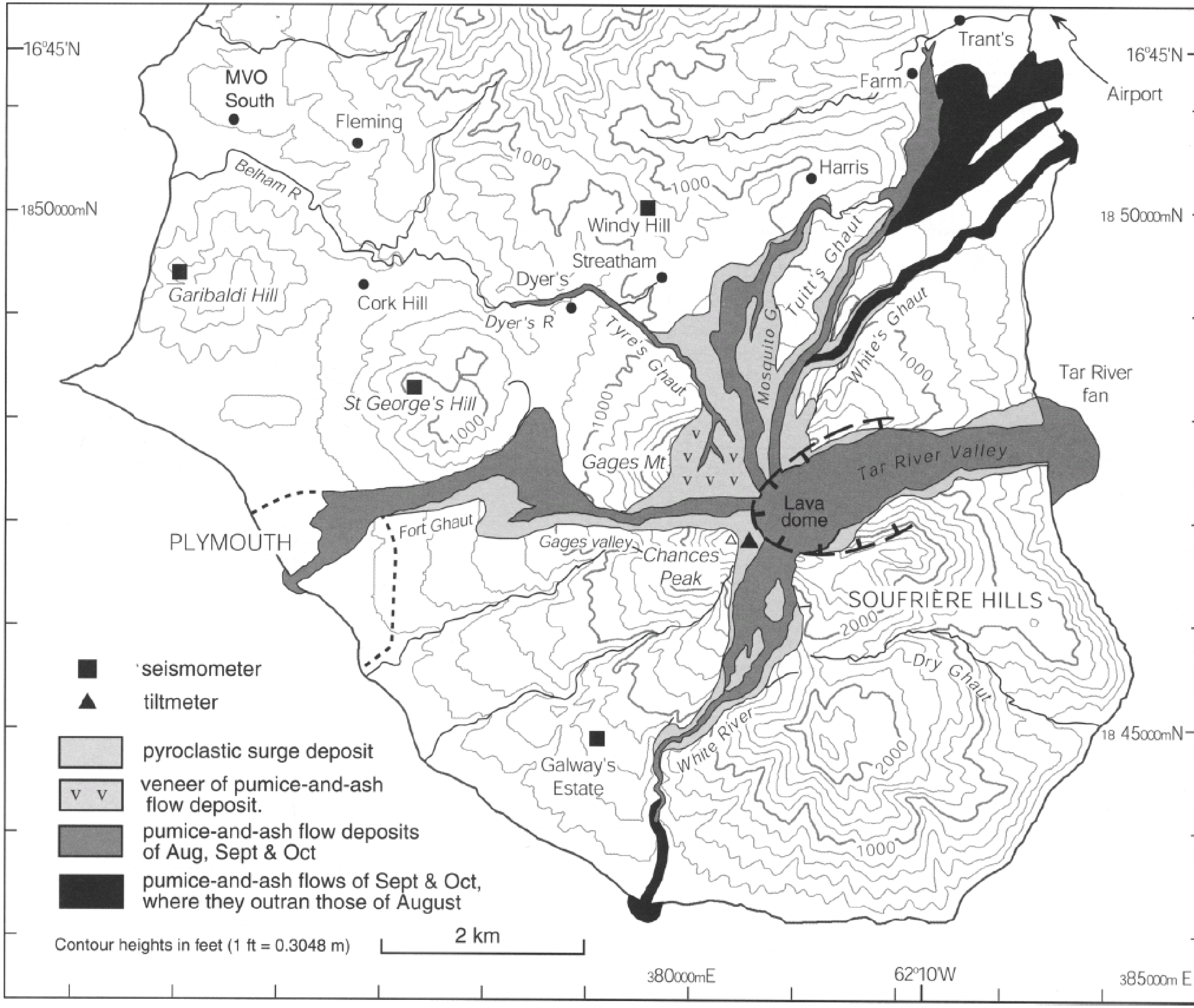

Fig. 5. Map showing the distribution of pumice-and-ash flow deposits formed during Vulcanian explosions in August 1997 and between 22 September and 21 October 1997, adapted from Druitt *et al.* (2002*b*).

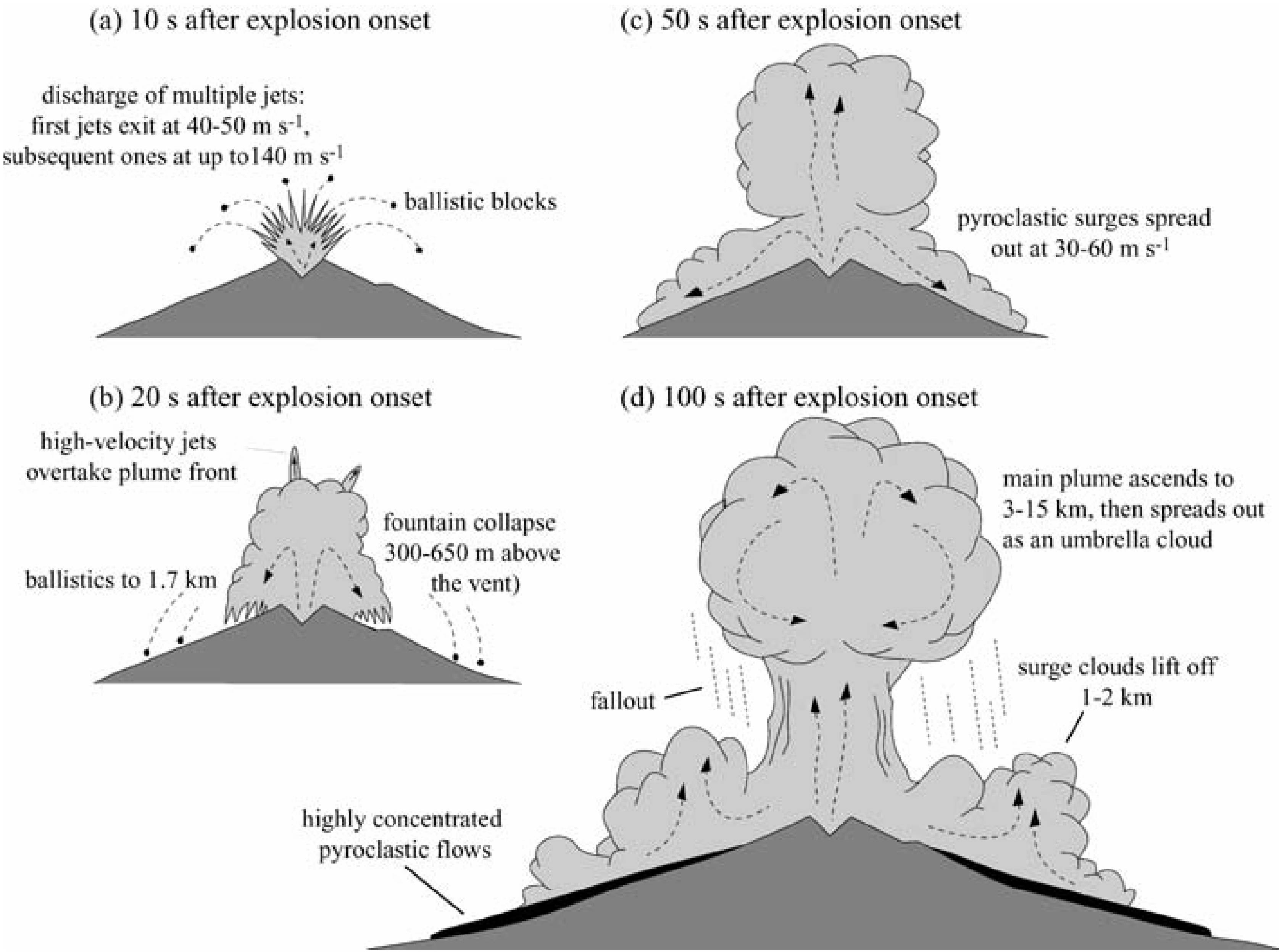

Druitt et al. 2002; Formenti et al. (2003)

Cyclic patterns of edifice deformation, hybrid seismicity, & explosions

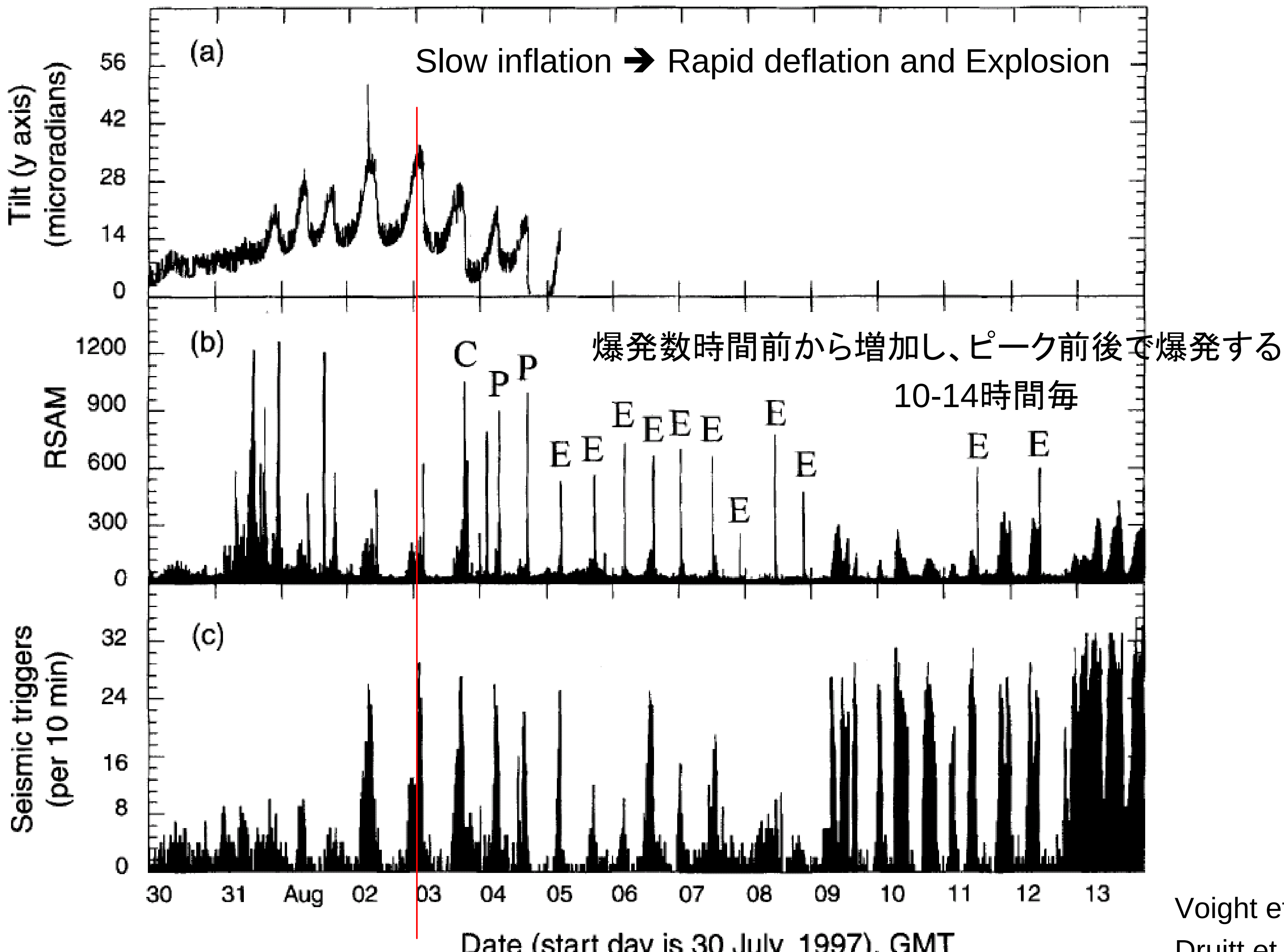

Voight et al. 1998

Druitt et al. 2002

Seismic signals during explosion

Phase 1: Long period (10-20 s duration)
Phase 2: Higher amplitude (a few min)
Phase 3: Harmonic tremor (1-3 hours)

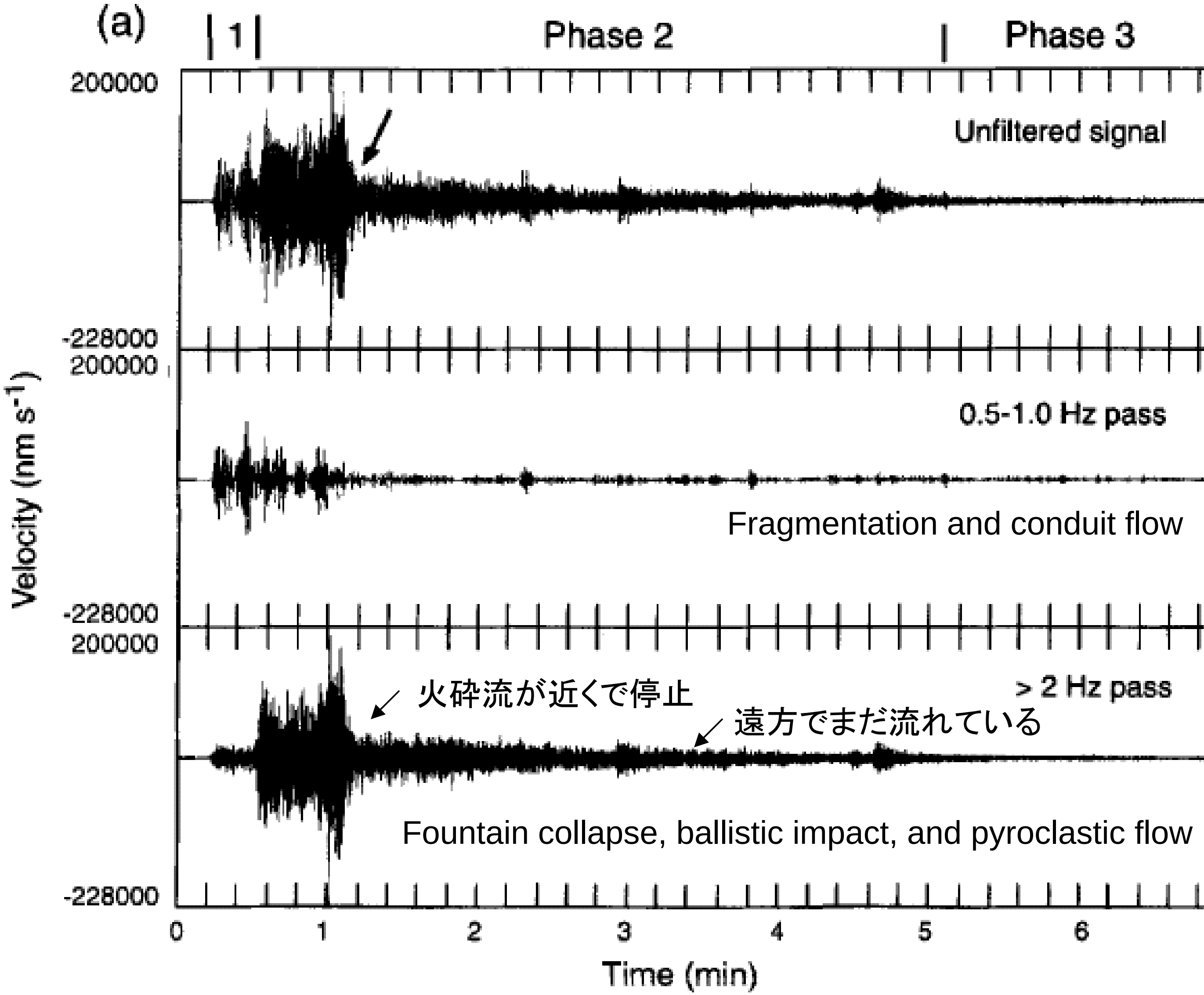

Druitt et al. 2002

Seismic signals during explosion

Enlargement of the first 1.4 minutes

Phase 1: Long period (10-20 s duration)

Phase 2: Higher amplitude (a few min)

Phase 3: Harmonic tremor (1-3 hours)

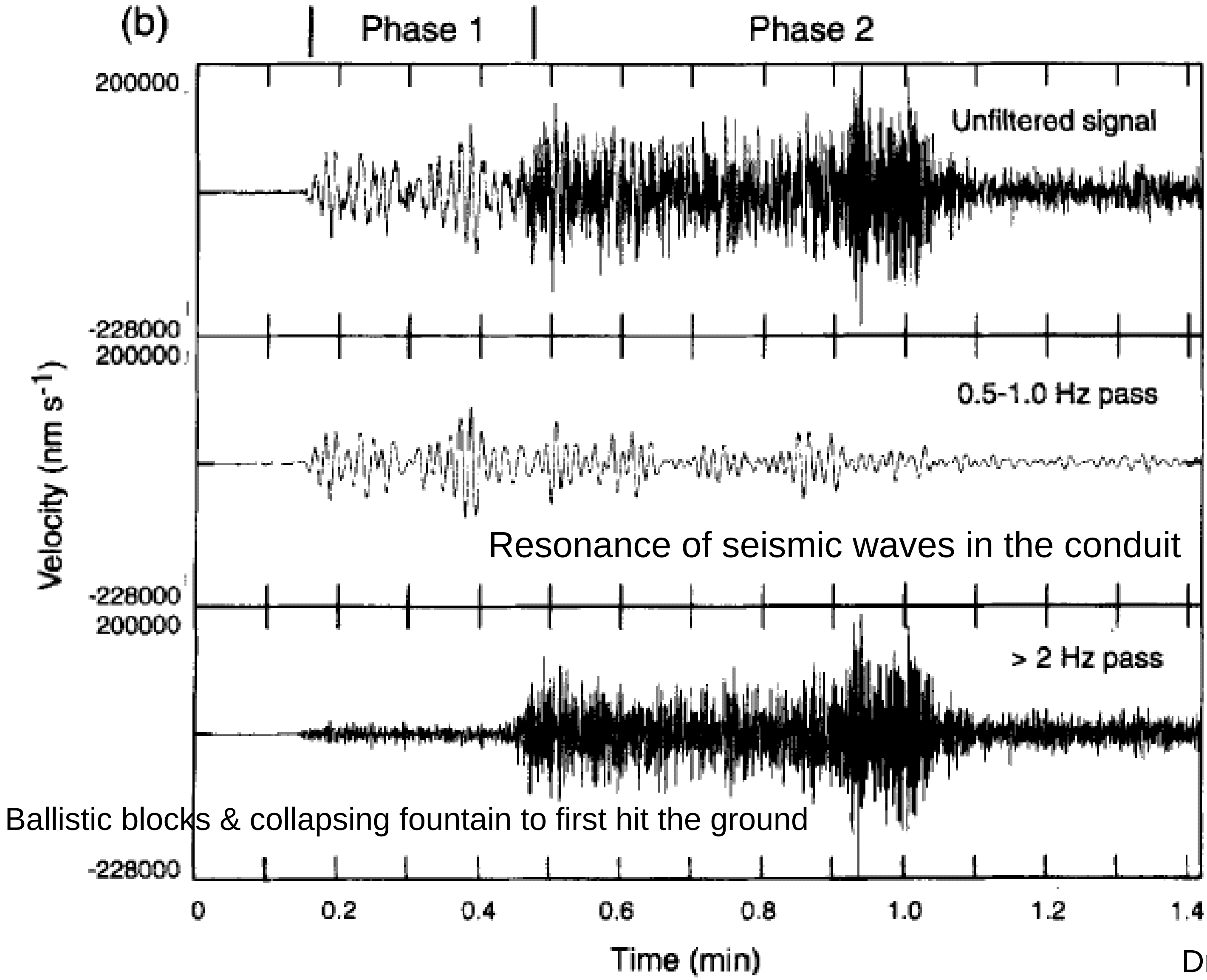

Druitt et al. 2002

Table 2. *The 12:05 explosion of 7 August 1997*

Time (s)	Event
0	**Start of explosion seismic signal (phase 1)***
1	Emergence of explosion jet 1 at $95 \pm 10\,m\,s^{-1}$
7	Emergence of explosion jet 2 at $95 \pm 10\,m\,s^{-1}$
17	Emergence of explosion jet 3 at $\geq 130\,m\,s^{-1}$
17.4	Fallout visible behind Gages Mountain from MVO South
18	**Start of seismic signal from fountain collapse and pyroclastic flows (phase 2)**
19.1	Fallout curtain descending over the north flank
21.6	First ballistics hit Farrell's Plain, 1.2 km north of the vent
22.0	First ballistics hit Paradise Plain, 1.2 km north of the vent
22.2	Collapsing fountain hits the north flank
22.8	Pyroclastic surge visible behind Gages Mountain
26.9	Ballistics reach maximum range on Paradise Plain, 1.6 km north of the vent
27.8	Pyroclastic surge in Mosquito Ghaut, 1.7 km from source, travelling at *c.* $45\,m\,s^{-1}$
27.9	Jet 3 arrives at the top of the plume
34.3	Pyroclastic surge passes Gages soufrière on the west flank
45	Pyroclastic surge ramps over Gage's Mountain and lofts
58	Pyroclastic surge reaches maximum runout on the Farrell's Plain and begins to loft
70	**Drop in intensity of the phase 2 seismic signal**
108	Pyroclastic flows reach the foot of St George's Hill on the west flank
167	Pyroclastic flow reaches the Paradise River, 3.5 km from source, at $10\,m\,s^{-1}$
187	Pyroclastic flow level with Harris, 3.4 km from source, at $9\,m\,s^{-1}$
202	Pyroclastic flow reaches sea on Tar River delta, 3.3 km from source, at $13–25\,m\,s^{-1}$
300	**End of pyroclastic flow seismic signal; continuing tremor (phase 3)**
c. 3600	End of the explosive eruption

* The seismic signal was measured at the Galway's Estate station (Fig. 10). The time for seismic waves to reach this station from the dome was about 1.5 s, so emergence of jet 1 occurred about 2.5 s after the onset of the explosion seismic activity.

Phase 1

Phase 2

Phase 3

Druitt et al. 2002

Vulcanian explosion の特徴

周期的な爆発:

- 2.5 〜 63 時間毎 (平均: 10 時間)
- Repeated slow inflation (増圧過程) & rapid deflation (減圧過程)

➔ Cyclic deformation of dome by stick-slip effect (Voight et al. 1999 etc.)

- Hybrid-earthquake ➔ hydro-fracturing & gas flow in rock or crystal-rich magma (Neuberg et al., 1998; Voight et al., 1999)

爆発に伴う地震波形:

- Low frequency: 0.5 〜 1 Hz (Phase 1 -3?)

  ➔ Vibrational response of the magmatic conduit to explosion itself (Neuberg & O'Gorman, 2002)

- High frequency: > 2 Hz (Phase 2)

  ➔ Combination of fountain collapse, ballisitc impact, pyroclastic flow (Miller et al., 1998; Uhira et al., 1994)

Summary of a single explosive cycle in 1997

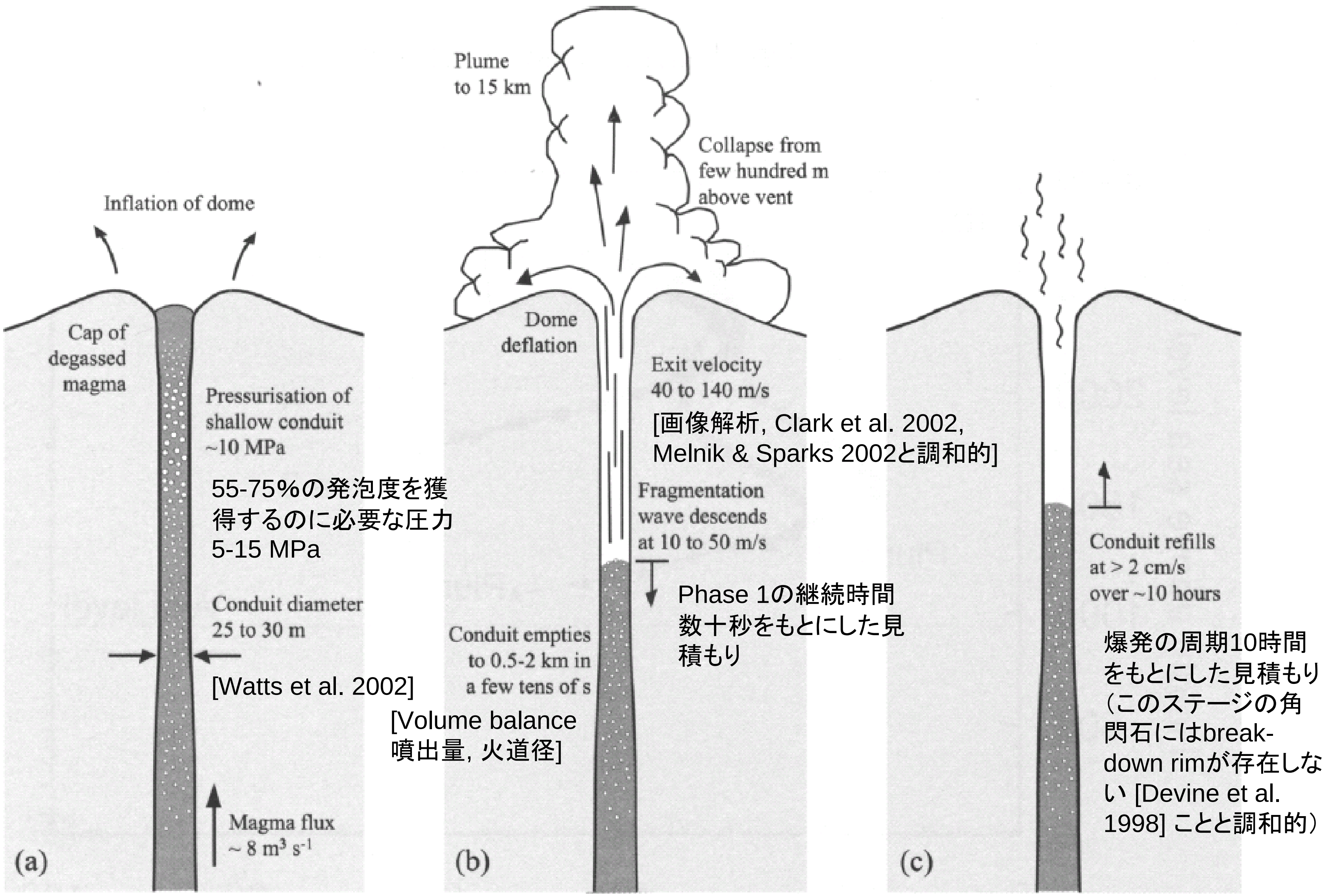

(Druitt et al., 2002, Formenti et al., 2003)

Calder et al. 1999

Inundated area

Geometric mobility parameter

Plane-shape parameter (=A/L²)

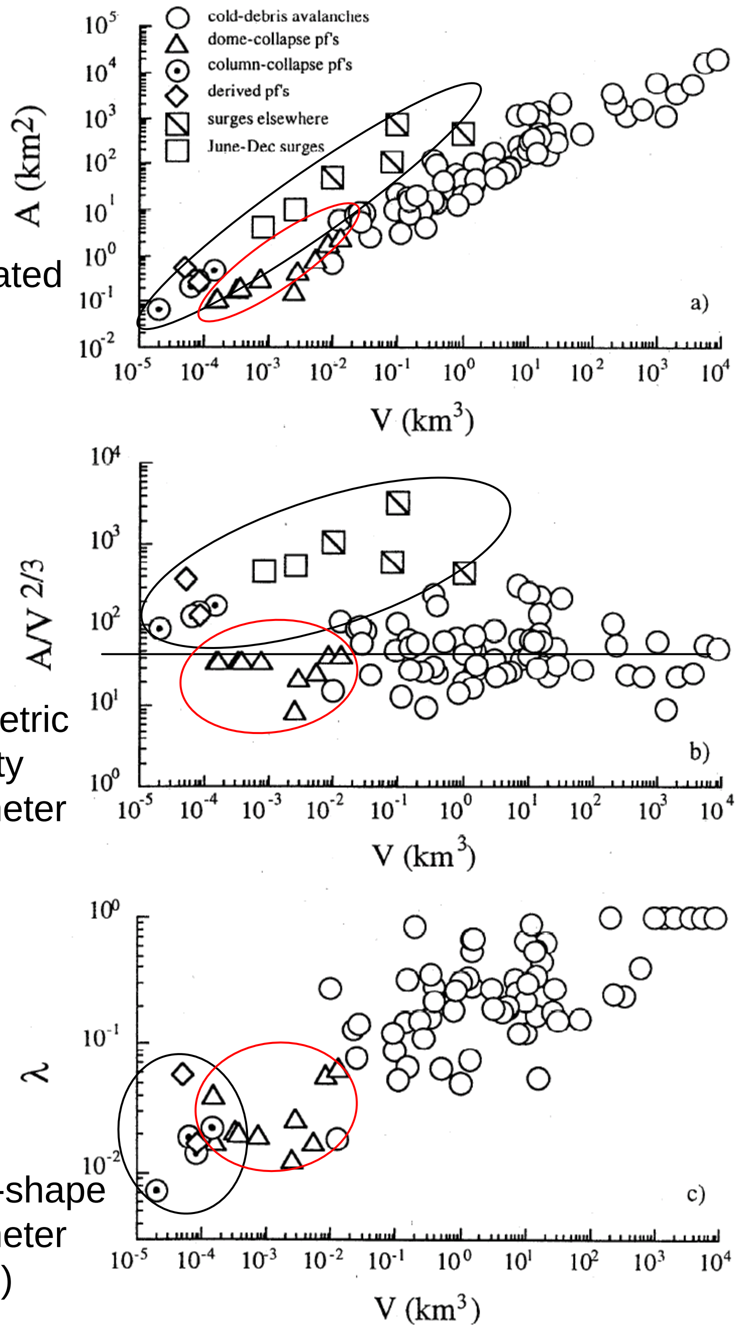

- Column-collapse pyroclastic flow
- Derived (secondary) pyroclastic flow
-Surges
の Mobility は、Block & ash flow より大きい傾向にある.

考えられる要因:

➔ 希薄・混濁状態の流れから火砕物が急速に堆積するため(流走に伴い、底面摩擦抵抗が小さい流動的なFlowへと変化していく)。[Rapid sedimentation from the dilute suspensions, which forms mobile concentrated underflows with low frictional resistance.]

➔ 細粒粒子を多く含むため [Finer-grained character] 。(この論文が発表された時点では、まだメカニズムについて言及されていないが、最近、Fine の役割の重要性について報告されている; Phillips et al. 2006 EPSL; Druitt et al. 2007 JVGR など。)

1996-1999年 Soufriere Hills 噴火のマグマについてのまとめ

Crystal-rich andesite (58.5-60.6 wt% SiO_2) (Murphy *et al.* 1998, 2000)

斑晶 [Phenocryst assemblage]: 斜長石 [Plagioclase] (28-30 vol%), 角閃石 [Amphibole] (3-10 vol%), 斜方輝石 [Orthopyroxene] (2-5 vol%), 石英 [Quartz], and 磁鉄鉱など [Oxides].

Crystal content

- Rapidly erupted lava (Murphy *et al.* 1998):

65-75 vol%: 斑晶 35-50 vol%; マイクロライト (<80 μm) 20-25 vol%.

25-35 vol%: high-SiO_2 rhyolite glass (76-80 wt% SiO_2).

- Slowly erupted lava (Barclay *et al.* 1998; Murphy *et al.* 2000)

Glass content 5-15 vol% (マイクロライトの晶出のためGlass量は減少する).

Water content of initial melt phase (Barclay *et al.* 1998; Murphy *et al.* 2000)

- 4-5 % water at 5-6 km depth (マグマ全体の含水量に換算して約 1.6 wt%).

Rheological properties (Sparks *et al.* 2000)

- Crystal-rich magma (25-35 vol% melt with 4-5 wt% H_20) ➔ Viscosity 10^6 Pas.
- Degassed crystalline lava (5-15 vol% melt) ➔ Viscosity 10^{14} Pas.

Available online at www.sciencedirect.com
SCIENCE DIRECT
Earth and Planetary Science Letters 214 (2003) 561–574
EPSL
www.elsevier.com/locate/epsl

Vesicle connectivity in pyroclasts and implications for the fluidisation of fountain-collapse pyroclastic flows, Montserrat (West Indies)

Y. Formenti [a,b,*], T.H. Druitt [a]

[a] Laboratoire Magmas et Volcans, Université Blaise Pascal-CNRS, 5 rue Kessler, 63038 Clermont-ferrand, France
[b] School of Earth Sciences, University of Leeds, Leeds LS2 9JT, UK

Received 19 February 2003; received in revised form 18 June 2003; accepted 8 July 2003

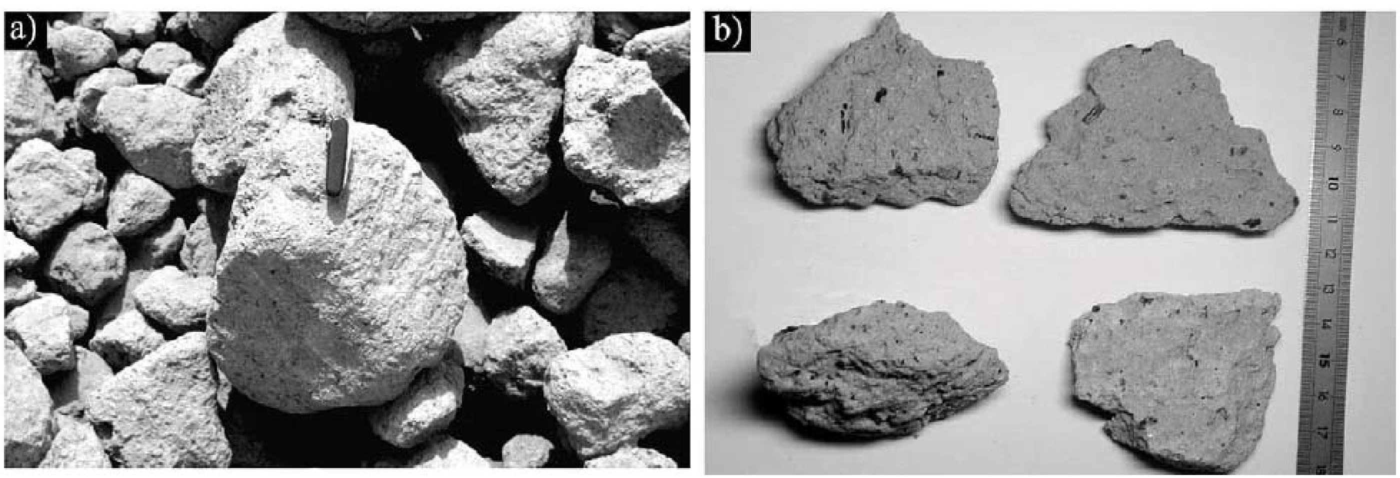

Fig. 2. (a) Typical pumice block in a fountain-collapse pyroclastic flow deposit from the 1997 Vulcanian explosions on Montserrat. The block is rounded due to attrition in the flow. (b) Fallout pumices generated by the same Vulcanian explosions in 1997. The angular, tabular shapes show that fragmentation in the conduit occurred by brittle spallation of a gas-pressurised magmatic foam [9].

軽石と溶岩塊の密度・発泡度

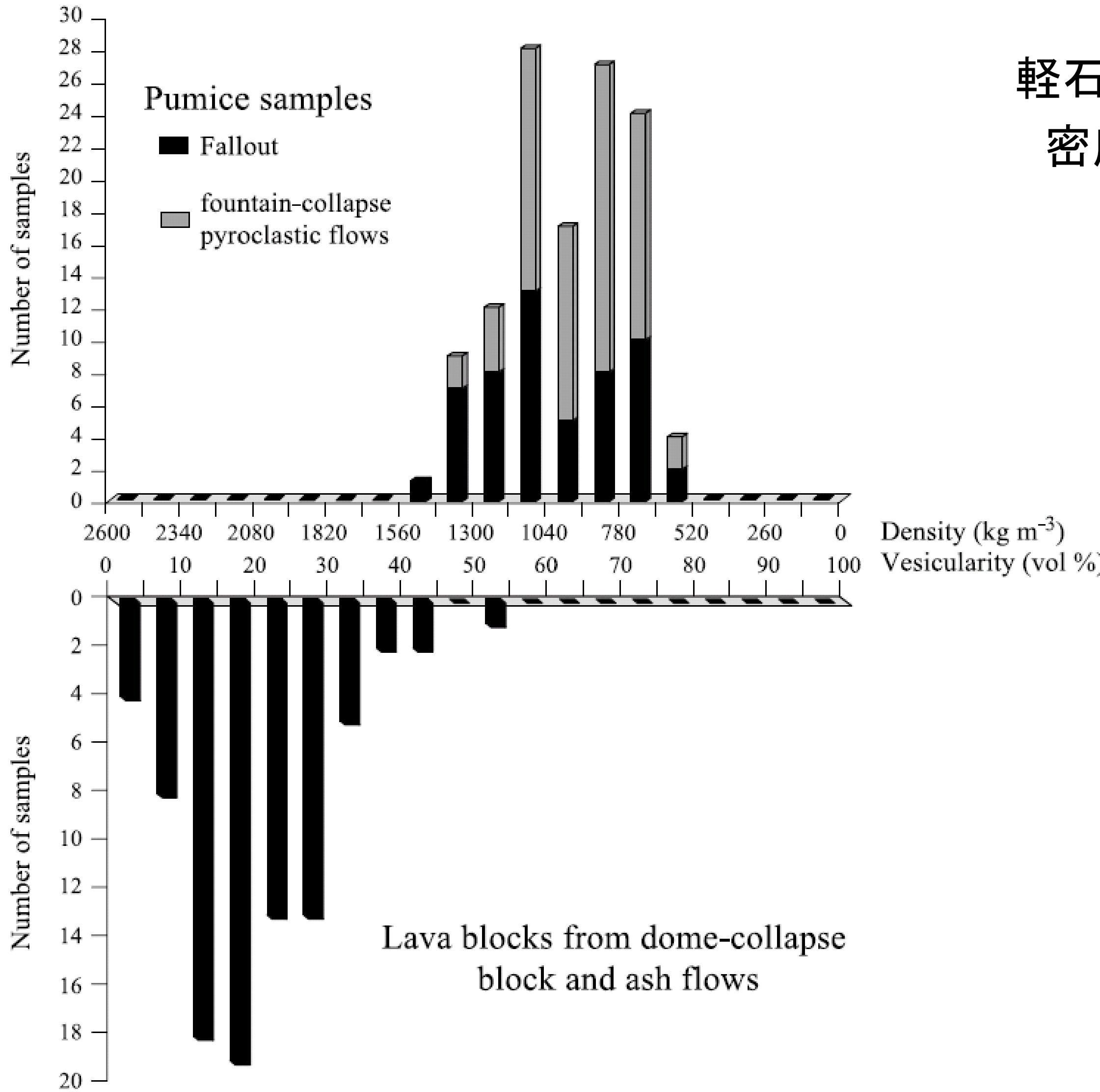

Fig. 1. Densities of pumices and lava blocks from Soufrière Hills Volcano: 85 lava blocks from the 21 September 1997 dome-collapse pyroclastic flows and 120 pumice blocks from the 1997 Vulcanian products (fountain-collapse pyroclastic flow deposits and associated fallout). Samples were dried and weighed, then placed into water to saturate the pores. They were then lightly dabbed to remove surface water and placed again in water to measure the external volume. Vesicularities were calculated using a mean density of 2600 kg m^{-3} for the solid phases.

Formenti and Druitt (2003)

火砕物粒子の密度・発泡度の定義とその関係

で示した部分の密度・体積(測定可能)について考える

連結 [連続] 気泡(connected vesicle)

独立気泡(isolated vesicle)この論文で重要視している

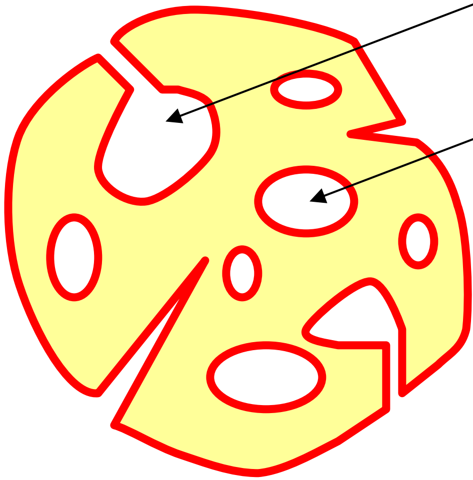

真密度(全ての空隙を除いた部分の密度)
➔ 粉末状にすると測定できる(発泡度0の状態)

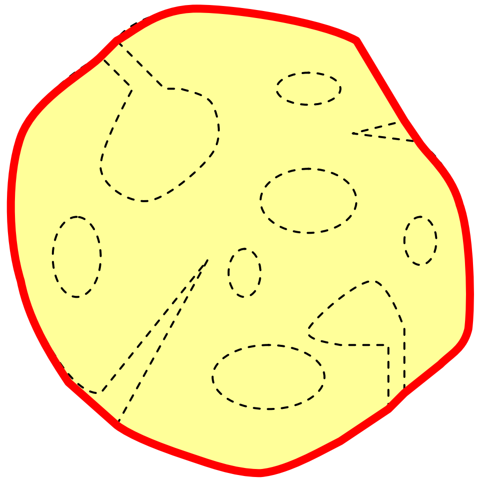

見かけ密度(全ての空隙を含んだ密度)
➔ 真密度を用いると全体の発泡度(連結気泡+独立気泡)が求まる

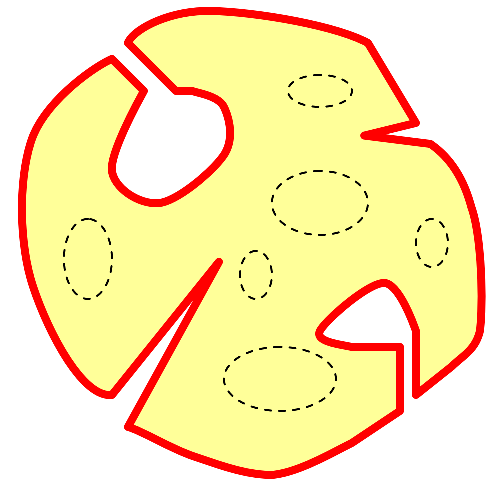

粒子密度(独立気泡を含む密度)
➔ 真密度を用いると連結気泡の割合が求まる

Connected vesicularity vs. Total vesicularity

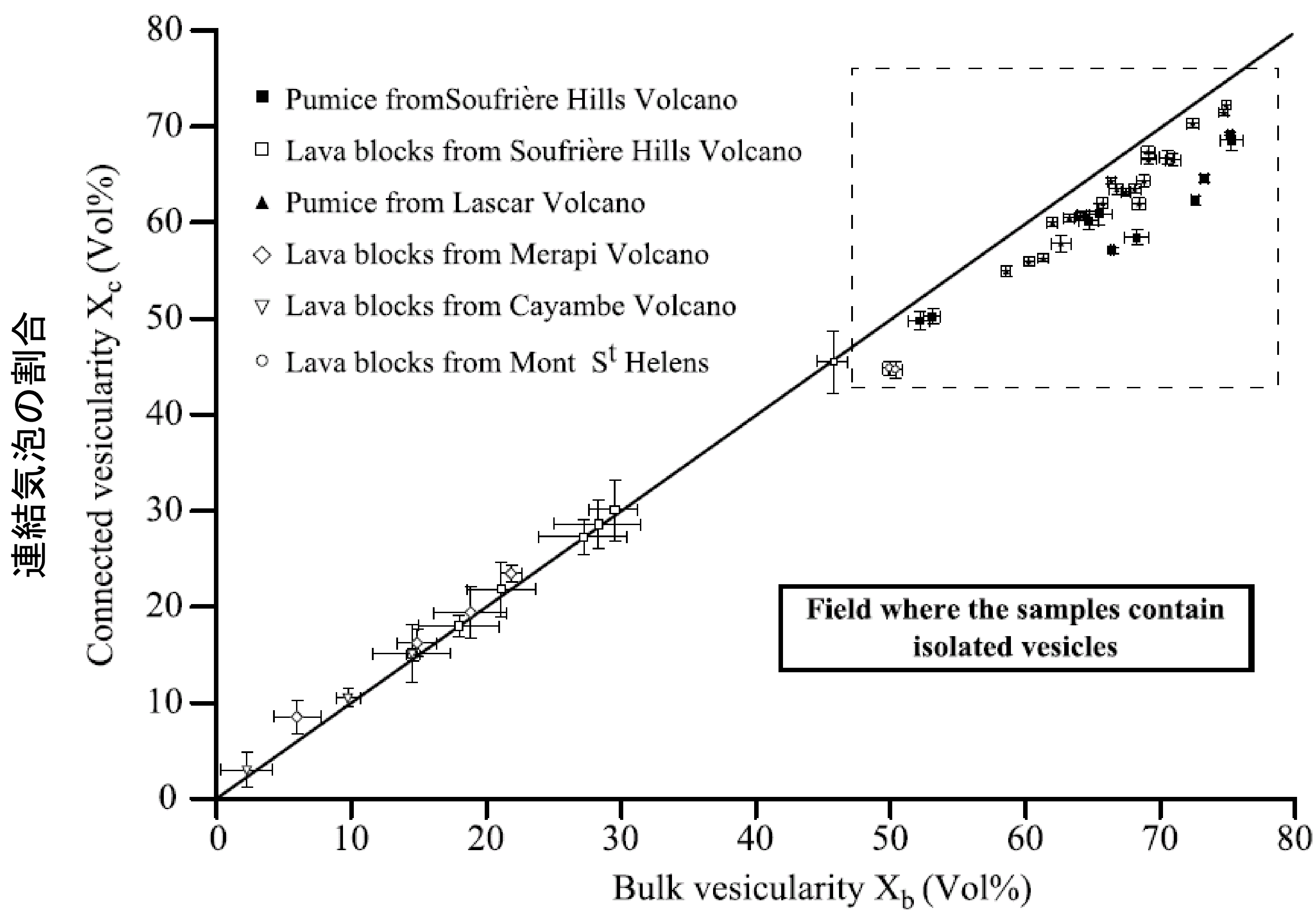

全体の発泡度（連結気泡＋独立気泡）

Formenti and Druitt (2003)

Vesicle textures

Fountain-collapse derived pumice

Large vesicle (15-50 μm) 45 %

➔ interconnected, ductile coalescence

Small vesicle (1-15 μm) 15 %

➔ Not connected, Large vesicleの間,

Spherical clusters, 2/3 が隔絶している

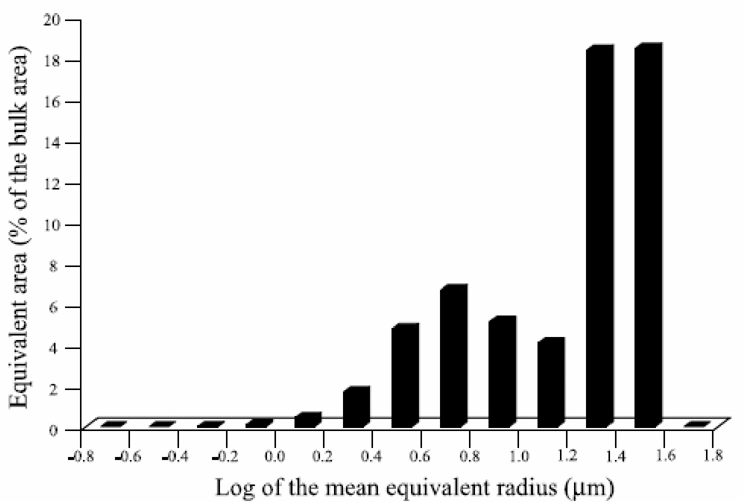

Dome-collapse derived pumice

ネットワークを形成している

Lascar pumice

Deflation after inflation

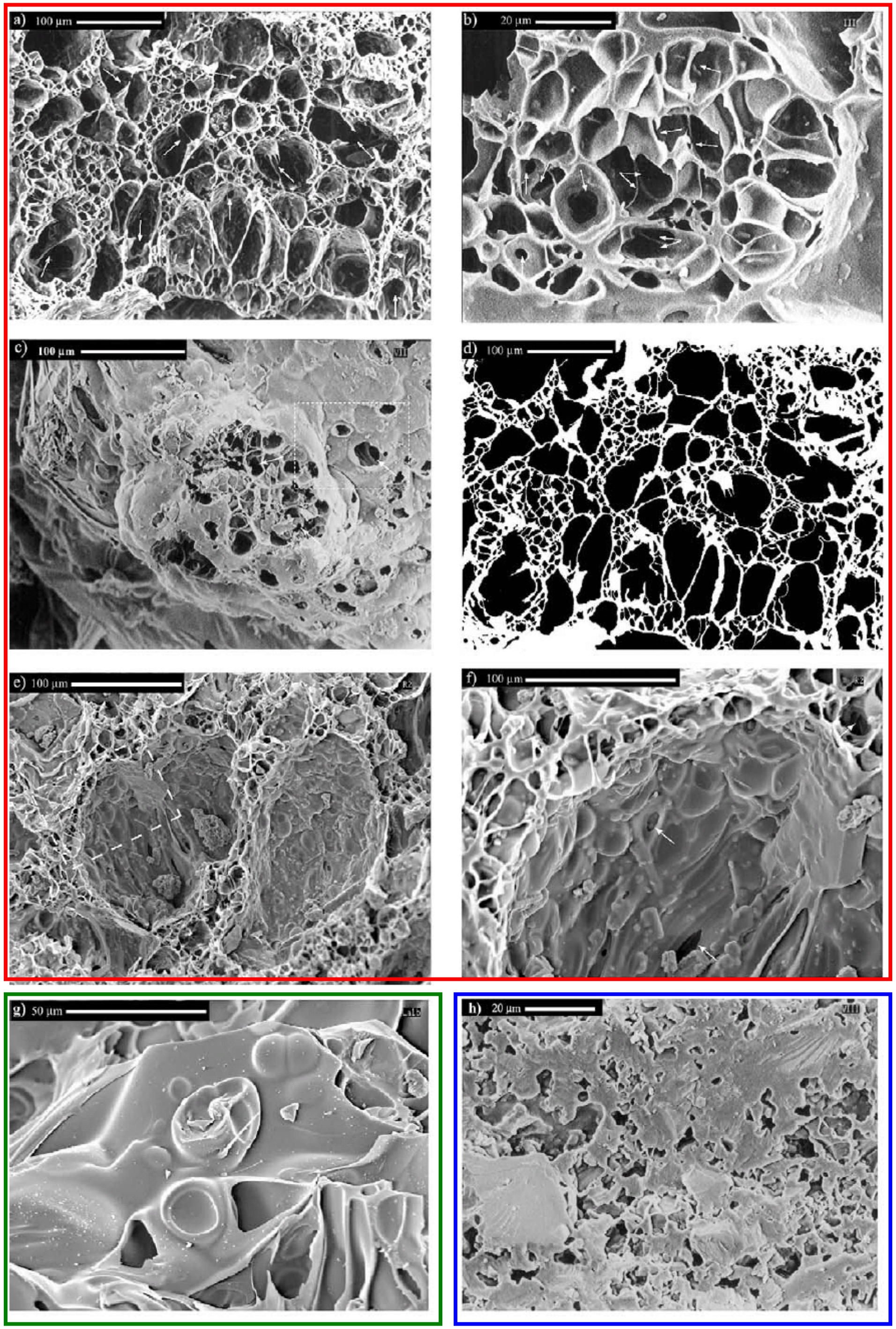

Vesicle bimodality の原因は？

２回の核形成イベントに対応

(1) Large vesicles: マグマ上昇時の初期

(2) Small vesicles: 最後の方。

可能性1: Fragmentation前のマイクロライト成長時。

可能性2: Fragmentation による減圧過程。

モデル計算を行うと、小さな気泡の成長は、噴出物が火道を出るまでの間に起こり得る.

➔ 直径15μm 成長するのに10 秒程度 ≒ Fragmentation level 1 km / 噴出速度 100 m/s [10 秒程度]

噴出後:

Large network-forming vesicle

→ ガスを放出してしまう

Small isolated vesicle

→ ガス圧を維持する

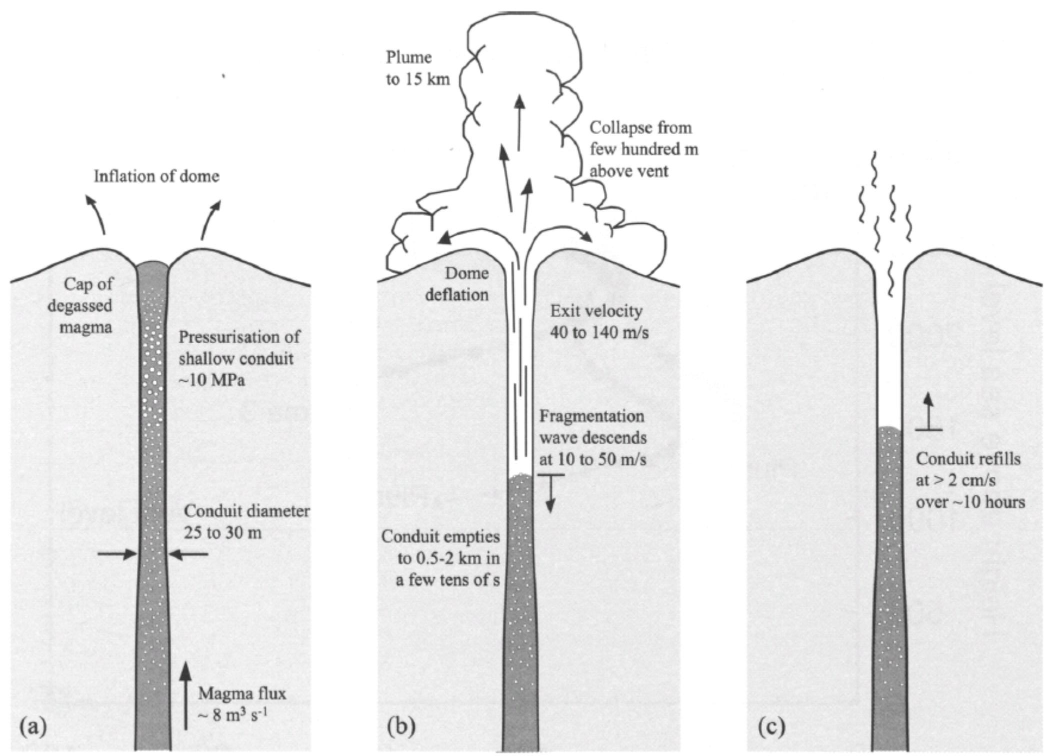

ガスの役割：　火砕流は流動化できるだけのガス量・ガス流速を獲得できたのか？

火砕流の流走中に放出されるガス量：

$$V_{gas-released} = \frac{P}{P_a} XYV_t$$

V_t: 火砕物に含まれる全ガス量, X: ratio of attrition (摩滅の割合),
Y: fraction of isolated vesicles（独立気泡の割合）

<u>火砕流内部で軽石の摩滅により発生するガスの流速（流動化の指標）vs. 独立気泡内部のガス圧</u>

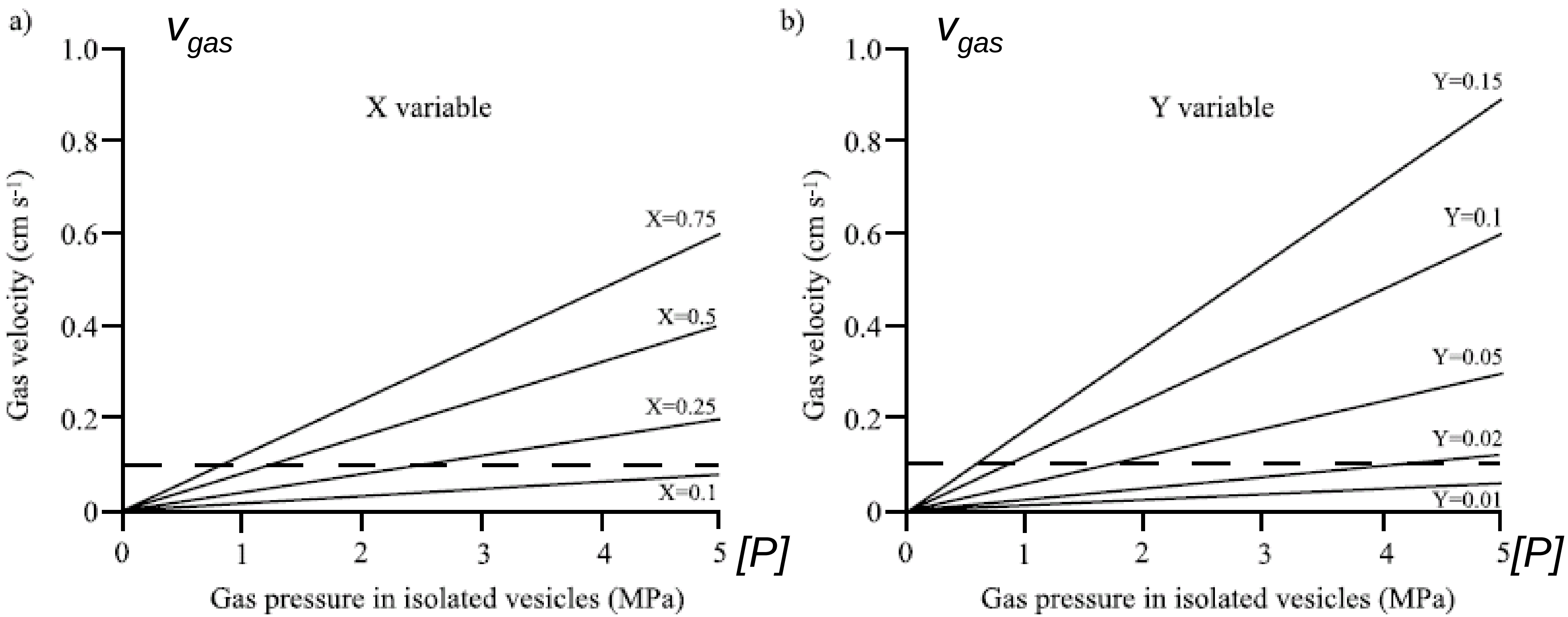

$$v_{gas} = \frac{V_{gas-released}}{tA} = \frac{XYV_t}{tA}\frac{P}{P_a}$$

t: 流走時間, A: 堆積面積（火砕流基底部の面積）

Formenti and Druitt (2003)

Fountain-collapse flow の特徴と成因について

独立気泡のRuptureによるガス放出が火砕流の流動化を促した可能性。

Exsolutionによるガス放出はそれほど重要でない（Flowの冷却が速く、ガスは拡散しきれないため）。

最も流動性（Mobility）の高い二次火砕流については、細粒粒子の存在や、より高いガス圧の獲得など、他の要因も考えられる。

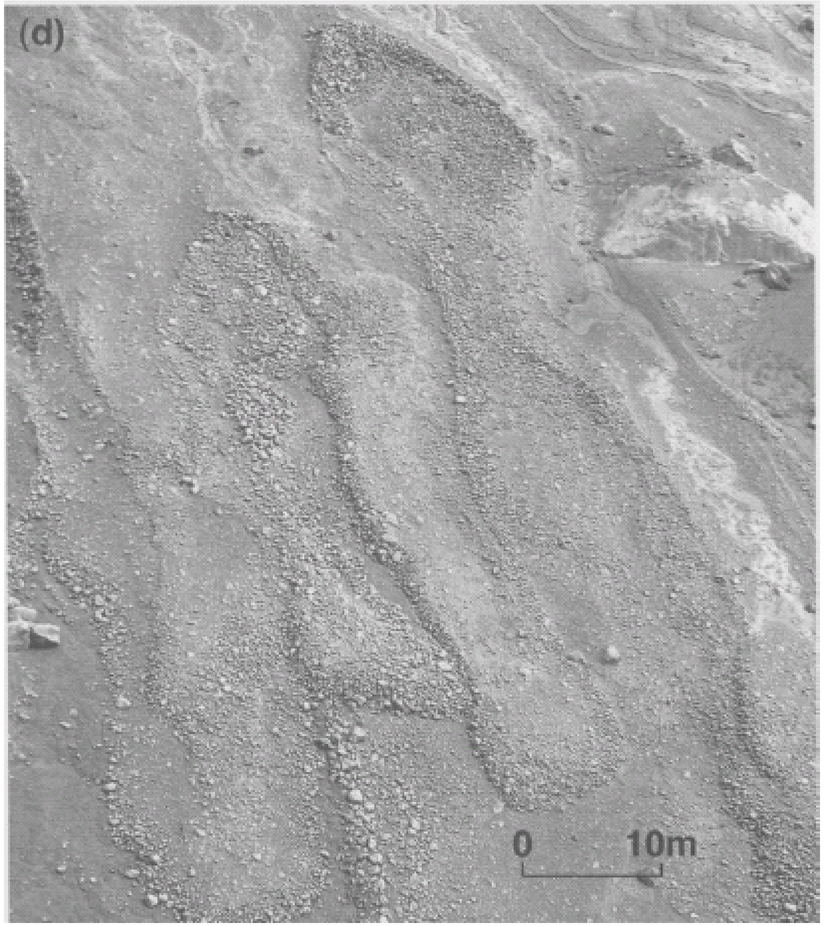

Appendix A：　Soufriere Hills 噴火のマグマについてのまとめ　References

Barclay et al. (1998) Experimental phase equilibria constraints on pre-eruptive storage conditions of the Soufriere Hills magma, GRL.

Devine et al. (1998) Petrologic determination of ascent rates for the 1995 - 1997 Soufriere Hills Volcano andesitic magma, GRL.

Devine et al. (1998) Petrologic evidence for pre-eruptive pressure-temperature conditions, and recent reheating, of andesitic magma erupting at the Soufriere Hills Volcano, Montserrat, W.I., GRL.

Murphy et al. (1998) The role of magma mixing in triggering the current eruption at Soufriere Hills Volcano, Montserrat, West Indies. GRL

Murphy et al. (2000) Remobilization of andesite magma by intrusion of mafic magma at the Soufriere Hills Volcano, Montserrat, West Indies. J. Petrology, 41, 21-42.

Couch, S., Harford, C.L., Sparks, R.S.J., Carroll, M.R., 2003a. Experimental constraints on the conditions of formation of highly calcic plagioclase microlites at the Soufrière Hills Volcano, Montserrat. J. Petrol. 44, 1455–1475.

Couch, S., Sparks, R.S.J., Carroll, M.R., 2003b. The kinetics of degassing-induced crystallization at Soufrière Hills Volcano, Montserrat. J. Petrol. 44, 1477–1502.

Buckley et al. (2006) Hornblende dehydration reactions during magma ascent at Soufriere Hills Volcano, Montserrat, Contrib Mineral Petrol.

Clarke et al. (2007) Petrologic constraints on the decompression history of magma prior to Vulcanian explosions at the Soufrière Hills volcano, Montserrat. JVGR.

Appendix B: Long-runout rockfalls (Dade and Huppert, 1998, Geology)

$$\delta\left(\frac{mU^2}{2}\right) = mg\delta z - \delta W$$

$$0 = mgH - W$$

$W = \tau AL$ ← The relaxation of stress during an earthquake (Knopoff, 1958)

$$W = \tau\left(\frac{A^3}{\lambda}\right)^{\frac{1}{2}}$$

$A = \lambda L^2$ The total area overrun by an avalanche and λ is the ratio of the average width to the length of an avalanche deposit.

τ: Average shear stress in the mobile debris

$$gmH = \tau\left(\frac{A^3}{\lambda}\right)^{\frac{1}{2}}$$

$$A = \lambda^{\frac{1}{3}}\left(\frac{\boxed{mgH}}{\tau}\right)^{\frac{2}{3}}$$

Potential energy

$$\frac{A}{V^{\frac{2}{3}}} = \lambda^{\frac{1}{3}}\left(\frac{\rho gH}{\tau}\right)^{\frac{2}{3}}$$

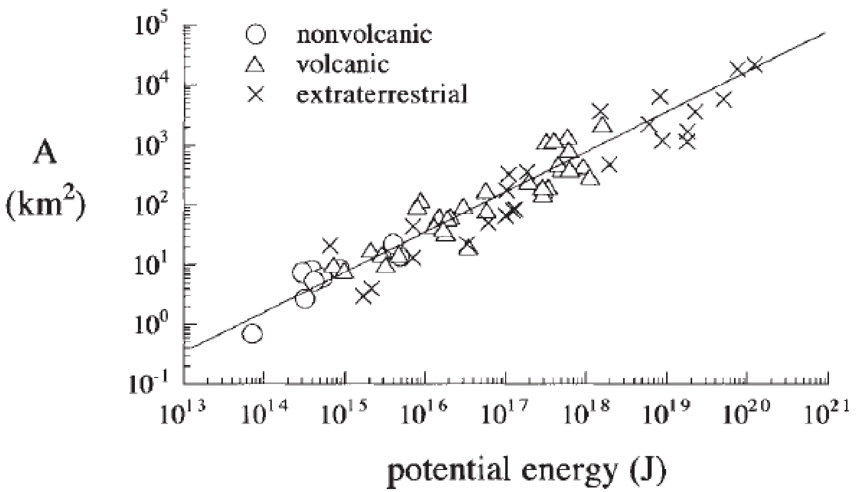

Figure 2. Area *A* overrun by avalanche or rockfall as function of potential energy *gHM* of debris before transport. Data are same as shown in Figure 1. Solid line indicates least-squares best fit of form given by text equation 5.